

1 **Distinct higher-order representations of natural sounds in human and ferret**
2 **auditory cortex**

3
4 **Authors**

5 Agnès Landemard*, Célian Bimbard*, Charlie Demené, Shihab Shamma, Sam Norman-
6 Haignere# and Yves Boubenec#

7 *, #: equal contribution

8
9 **Abstract**

10 Little is known about how neural representations of natural stimuli differ across species. Speech
11 and music for example play a unique role in human hearing, but it is unclear how auditory
12 representations of speech and music differ between humans and other animals. Using functional
13 Ultrasound imaging, we measured responses in ferret auditory cortex to a set of natural and
14 spectrotemporally-matched synthetic sounds previously tested in humans, as well as natural and
15 synthetic ferret vocalizations. Ferrets showed similar frequency and modulation tuning to that
16 observed in humans. But while humans showed selective responses to natural speech and music
17 in non-primary auditory cortex, ferret responses to natural and synthetic sounds were closely
18 matched throughout primary and non-primary regions, even when tested with ferret vocalizations.
19 This finding suggests the unique demands of speech and music have substantially altered higher-
20 order acoustic representations in human auditory cortex, while largely preserving lower-level
21 tuning for frequency and modulation.

22 Introduction

23
24 Surprisingly little is known about how sensory representations of natural stimuli differ across
25 species (Theunissen and Elie, 2014). This question is central to understanding how evolution and
26 development shape sensory representations (Moore and Woolley, 2019) as well as developing
27 animal models of human brain functions. Audition provides a natural test case because speech
28 and music play a unique role in human hearing (Zatorre et al., 2002; Hickok and Poeppel, 2007;
29 Patel, 2012). While human knowledge of speech and music clearly differs from other species
30 (Pinker and Jackendoff, 2005), it remains unclear how neural representations of speech and
31 music differ from those in other species, particularly within the auditory cortex. Few studies have
32 directly compared neural responses to natural sounds between humans and other animals, and
33 those which have done so, have often observed similar responses. For example, both humans
34 and non-human primates show regions that respond preferentially to conspecific vocalizations
35 (Belin et al., 2000; Petkov et al., 2008). Human auditory cortex exhibits selectivity for speech
36 phonemes (Mesgarani et al., 2014; Di Liberto et al., 2015), but much of this selectivity can be
37 predicted by simple forms of spectrotemporal modulation tuning (Mesgarani et al., 2014), and
38 perhaps as a consequence, can be observed in other animals such as ferrets (Mesgarani et al.,
39 2008; Steinschneider et al., 2013). Consistent with this finding, maps of spectrotemporal
40 modulation, measured using natural sounds, appear coarsely similar between humans and
41 macaques (Erb et al., 2019) although temporal modulations present in speech may be over-
42 represented in humans. Thus, it remains unclear if the representation of natural sounds in auditory
43 cortex differs substantially between humans and other animals, and if so, how.

44
45 A key challenge is that representations of natural stimuli are transformed across different stages
46 of sensory processing, and species may share some but not all representational stages.
47 Moreover, responses at different sensory stages are often correlated across natural stimuli (de
48 Heer et al., 2017), making them difficult to disentangle. Speech and music, for example, have
49 distinctive patterns of spectrotemporal modulation energy (Singh and Theunissen, 2003; Ding et
50 al., 2017), as well as higher-order structure (e.g. syllabic and harmonic structure) that is not well
51 captured by modulation (Norman-Haignere and McDermott, 2018). To isolate neural selectivity
52 for higher-order structure, we recently developed a method for synthesizing sounds whose
53 spectrotemporal modulation statistics are closely matched to a corresponding set of natural
54 sounds (Norman-Haignere and McDermott, 2018). Because the synthetic sounds are otherwise
55 unconstrained, they lack perceptually salient higher-order structure, particularly for complex
56 natural sounds like speech and music which are poorly captured by modulation statistics, unlike
57 many other natural sounds (McDermott and Simoncelli, 2011). We found that human primary
58 auditory cortex responds similarly to natural and spectrotemporally synthetic sounds, while non-
59 primary regions respond selectively to the natural sounds. Most of this selectivity is driven by
60 preferential responses to natural speech and music in distinct neural populations of non-primary
61 auditory cortex (Norman-Haignere et al., 2015; Norman-Haignere and McDermott, 2018).
62 Importantly, this response preference for natural speech and music is independent of speech
63 semantics, since similar responses are observed for native and foreign speech (Norman-Haignere
64 et al., 2015; Overath et al., 2015), and explicit musical training, since music selectivity is robust in
65 humans without any training (Boebinger et al., 2020). These findings suggest that human non-
66 primary regions respond selectively to higher-order acoustic features that both cannot be
67 explained by lower-level modulation statistics, but do not yet reflect explicit semantic knowledge.

68
69 The goal of the present study was to test whether such higher-order selectivity reflects a generic
70 mechanism for analyzing complex sounds like speech and music, and thus is present in other
71 species, or is instead driven by the unique demands of speech and music perception in humans.
72 We addressed this question by measuring cortical responses in ferrets – one of the most common

73 animal models used to study auditory cortex (Nelken et al., 2008) – to the same set of natural and
74 synthetic sounds previously tested in humans, as well as natural and synthetic ferret vocalizations.
75 Responses were measured using functional UltraSound imaging (fUS) (Macé et al., 2011;
76 Bimbard et al., 2018), a newly developed wide-field imaging technique that like fMRI detects
77 changes in neural activity via changes in blood-flow (movement of blood induces a doppler effect
78 detectable with ultrasound). fUS has substantially better spatial resolution than fMRI making it
79 applicable to small animals like ferrets. We found that tuning for spectrotemporal modulations
80 present in both natural and synthetic sounds was similar between humans and animals, and could
81 be quantitatively predicted across species, consistent with prior findings (Mesgarani et al., 2008;
82 Erb et al., 2019). But unlike humans, ferret responses to natural and synthetic sounds were similar
83 throughout primary and non-primary auditory cortex even when comparing natural and synthetic
84 ferret vocalizations; and the small differences that were present in ferrets were weak and spatially
85 scattered, unlike the selectivity observed in humans. This finding suggests that speech and music
86 have substantially altered higher-order cortical representations in humans, while preserving much
87 of the lower-level tuning for frequency and modulation.
88

89 **Results**

91 **Experiment I: Comparing ferret cortical responses to natural versus synthetic sounds**

92 We measured cortical responses with fUS to the same 36 natural sounds tested previously in
93 humans plus 4 additional ferret vocalizations (Experiment II tested many more ferret
94 vocalizations). The 36 natural sounds included speech, music, and other environmental sounds
95 (see **Table S1**). For each natural sound, we synthesized 4 sounds that were matched on acoustic
96 statistics of increasing complexity (**Fig 1A**): (1) cochlear energy statistics (2) temporal modulation
97 statistics (3) spectral modulation statistics and (4) spectrotemporal modulation statistics.
98 Cochlear-matched sounds had a similar frequency spectrum, but their modulation content was
99 unconstrained and thus differed from the natural sounds. Modulation-matched sounds were
100 additionally constrained in their temporal and/or spectral modulation rates, measured by linearly
101 filtering a cochleagram representation with filters tuned to different modulation rates (modulation-
102 matched sounds also had matched cochlear statistics in order to isolate the contribution of
103 modulation). For complex sounds like speech and music, the modulation-matched sounds audibly
104 differ from their natural counterparts likely because they lack higher-order structure, not captured
105 by spectrotemporal modulation statistics (listen to example sounds [here](#)). We focused on time-
106 averaged statistics because the hemodynamic response measured by both fMRI and fUS reflects
107 a time-averaged measure of neural activity. As a consequence, each of the synthetic sounds can
108 be thought of as being matched under a different model of the fUS or fMRI response (Norman-
109 Haignere and McDermott, 2018).
110

111 We measured fUS responses throughout primary and non-primary ferret auditory cortex (**Fig 1B**).
112 We first plot the response timecourse to all 40 natural sounds for one example voxel in non-
113 primary auditory cortex (dPEG) (**Fig 1C**). We plot the original timecourse of the voxel as well as
114 a denoised version computed by projecting the timecourse onto a small number of reliable
115 components, which we found substantially improved prediction accuracy in left-out data (see
116 Methods for details). As expected and similar to fMRI, we observed a gradual build-up of the
117 hemodynamic response after stimulus onset. The shape of the response timecourse was similar
118 across stimuli, but the magnitude of the response varied, and we thus summarized the response
119 of each voxel to each sound by its time-averaged response magnitude (the same approach used
120 in our prior fMRI study).

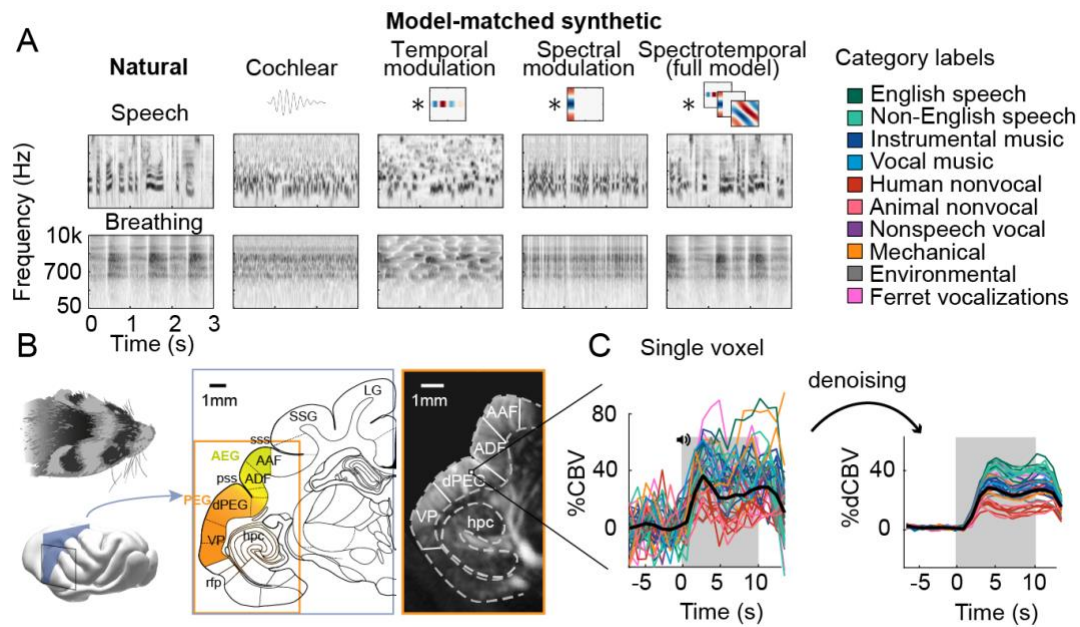
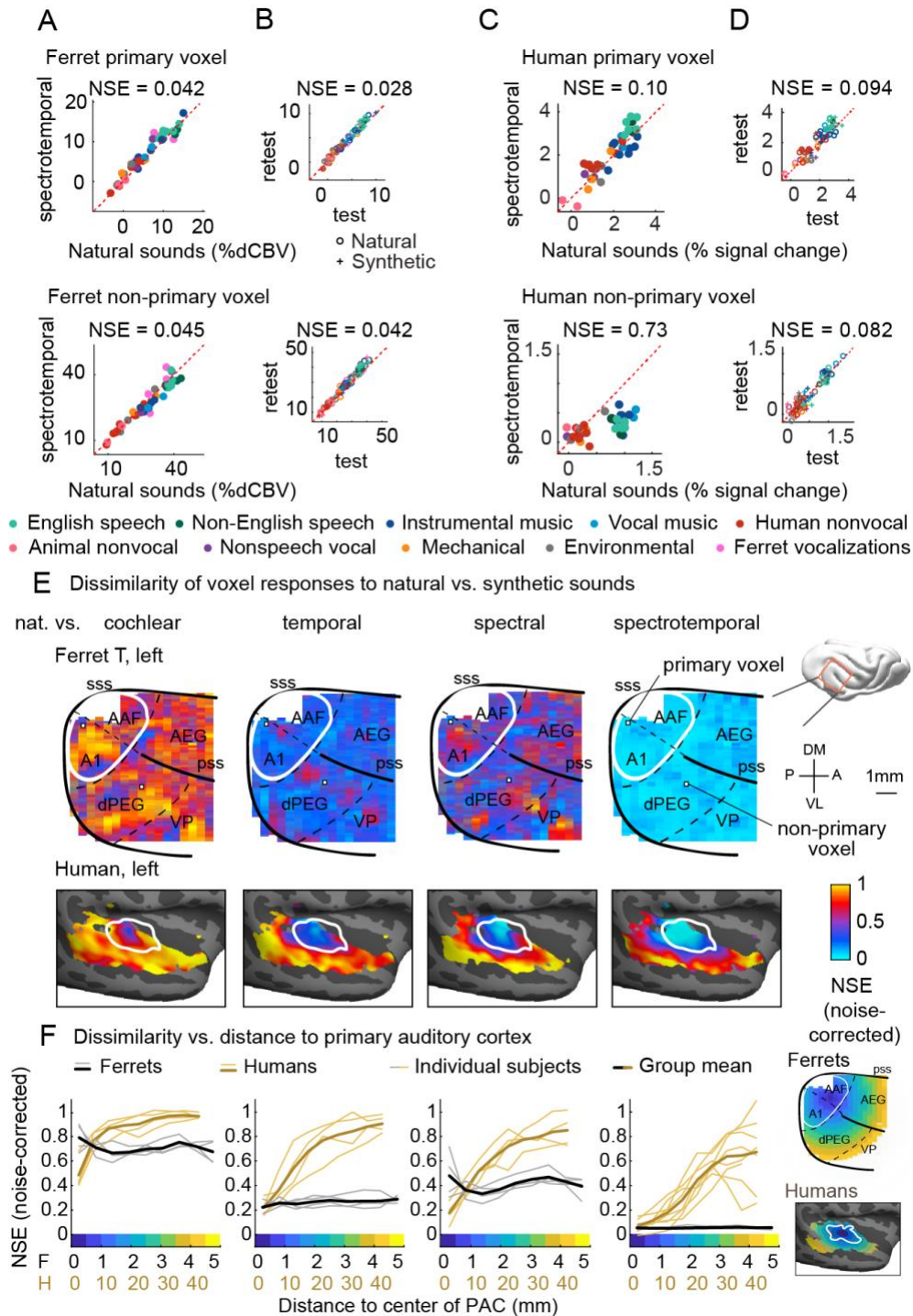


Figure 1. Schematic of stimuli and imaging protocol. **A**, Cochleagrams for two example natural sounds (left column) and corresponding synthetic sounds (right four columns) that were matched to the natural sounds along a set of acoustic statistics of increasing complexity. Statistics were measured by filtering a cochleagram with filters tuned to temporal, spectral or joint spectrotemporal modulations. The natural sounds were diverse, and were grouped into 10 different categories shown at right. English and Non-English speech are separated out because all of the human subjects tested in our prior study were native English speakers, and so the distinction is meaningful in humans. **B**, Schematic of the imaging procedure. A three-dimensional volume covering all of ferret auditory cortex was acquired through successive coronal slices. Auditory cortical regions (colored regions) were mapped with anatomical and functional markers. The rightmost image shows a single ultrasound image with overlaid region boundaries. Auditory regions: dPEG: dorsal posterior ectosylvian gyrus; AEG: anterior ectosylvian gyrus; VP: ventral posterior auditory field; ADF: anterior dorsal field; AAF: anterior auditory field. Non-auditory regions: hpc: hippocampus; SSG: suprasylvian gyrus; LG: lateral gyrus. Anatomical markers: pss: posterior sylvian sulcus; sss: superior sylvian sulcus. **C**, Response timecourse of a single voxel to all natural sounds, measured from raw (left) and denoised data (right). Each line reflects a different sound, and its color indicates the sound's category. The gray region shows the time window when sound was present. The location of this voxel corresponds to the highlighted voxel in panel B.

We next plot the time-averaged response of two example voxels – one in primary auditory cortex (A1) and one in a non-primary area (dPEG) – to natural and corresponding synthetic sounds that have been matched on the full spectrotemporal modulation model (**Fig 2A**). For comparison, we plot the test-retest reliability of each voxel across repeated presentations of the same sound (**Fig 2B**), as well as corresponding figures from two example voxels in human primary/non-primary auditory cortex (**Fig 2C-D**; these voxels are re-plotted from our prior paper). As in our prior study, we quantified the similarity of responses to natural and synthetic sounds using the normalized squared error (NSE). The NSE takes a value of 0 if responses to natural and synthetic sounds are the same, and 1 if there is no correspondence between the two (see Methods for details).



149
 150 **Figure 2: Dissimilarity of responses to natural vs. synthetic sounds in ferrets and humans.** **A**,
 151 Response of two example fUS voxels to natural and corresponding synthetic sounds with matched
 152 spectrotemporal modulation statistics. Each dot shows the time-averaged response to a single pair of
 153 natural/synthetic sounds (after denoising), with colors indicating the sound category. The example voxels
 154 come from primary (top, A1) and non-primary (bottom, dPEG) regions of the ferret auditory cortex. The
 155 normalized squared error (NSE) quantifies the dissimilarity of responses. **B**, Test-retest response of the
 156 example voxels across all natural (o) and synthetic (+) sounds (odd vs. even repetitions). The responses
 157 were highly reliable due to the denoising procedure. **C-D**, Same as panel A-B, but showing two example
 158 voxels from human primary/non-primary auditory cortex. **E**, Maps plotting the dissimilarity of responses to
 159 natural vs. synthetic sounds from one ferret hemisphere (top row) and from humans (bottom row). Each
 160 column shows results for a different set of synthetic sounds. The synthetic sounds were constrained by
 161 statistics of increasing complexity from left to right: just cochlear statistics, cochlear + temporal modulation
 162 statistics, cochlear + spectral modulation statistics, and cochlear + spectrotemporal modulation statistics.
 163 Dissimilarity was quantified using the normalized squared error (NSE), corrected for noise using the test-

164 retest reliability of the voxel responses. Ferret maps show a “surface” view from above of the sylvian gyri,
165 similar to the map in humans. Surface views were computed by averaging activity perpendicular to the cortical
166 surface. The border between primary and non-primary auditory cortex is shown with a white line in both
167 species, and was defined using tonotopic gradients. Areal boundaries in the ferret are also shown (dashed
168 thin lines). This panel shows results from one hemisphere of one animal (Ferret T, left hemisphere), but
169 results were similar in other animals/hemispheres (**Fig S1**). The human map is a group map averaged across
170 many subjects, but results were similar in individual subjects (Norman-Haignere and McDermott, 2018). **F**,
171 Voxels were binned based on their distance to primary auditory cortex (defined tonotopically). This figure
172 plots the median NSE value in each bin. Each thin line corresponds to a single ferret hemisphere (gray) or a
173 single human subject averaged across hemispheres (gold) (results were very similar in the left and right
174 hemisphere of humans). Thick lines show the average across all hemispheres/subjects.
175

176 Both the primary and non-primary ferret voxels produced nearly identical responses to natural
177 and corresponding synthetic sounds (NSEs: 0.042, 0.045), suggesting that spectrotemporal
178 modulation are sufficient to account for the responses in these voxels. The human primary voxel
179 also showed similar responses to natural and synthetic responses, and the NSE for natural vs.
180 synthetic sounds (0.1) was similar to the test-retest NSE (0.094), indicating that the response was
181 about as similar as possible given the noise ceiling. In contrast, the human non-primary voxel
182 responded selectively to the natural speech (green) and music (blue), yielding a high NSE value
183 (0.73). This pattern demonstrates that spectrotemporal modulations are insufficient to drive the
184 response of the human non-primary voxel, plausibly because it responds to higher-order features
185 that are not captured by modulation statistics.
186

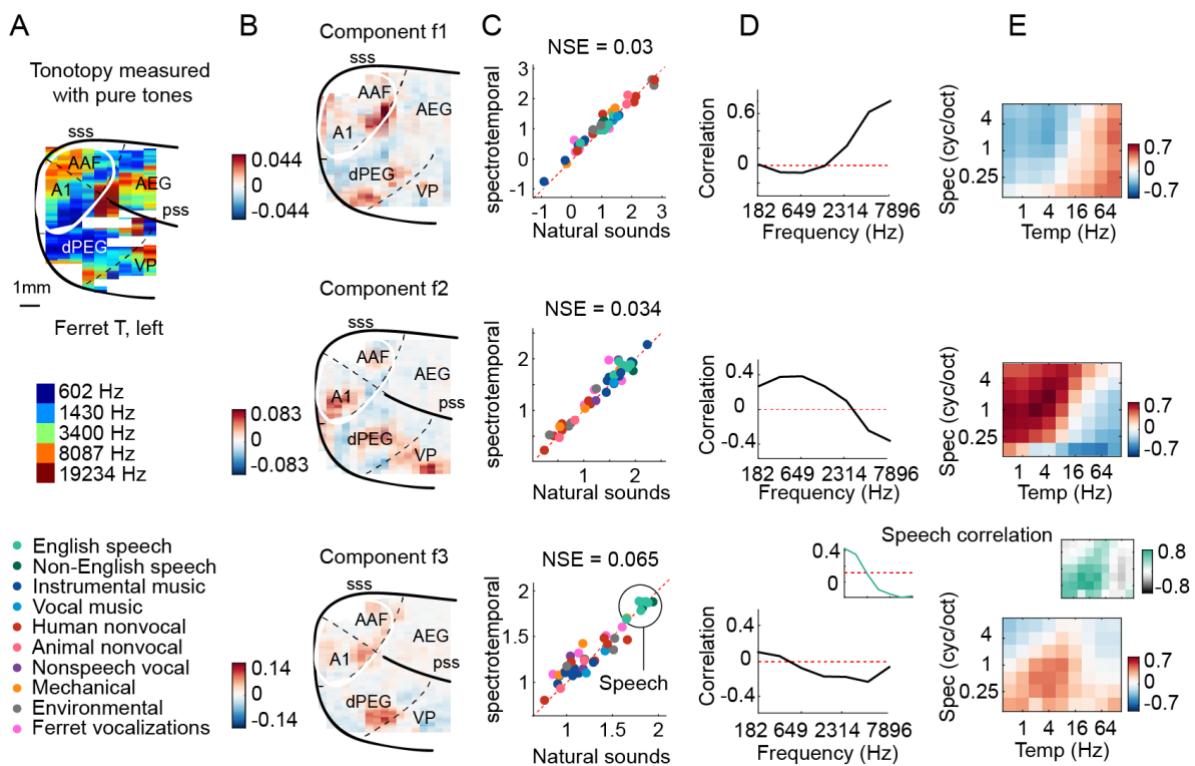
187 We quantified this trend across voxels by plotting maps of the noise-corrected NSE between
188 natural and synthetic sounds (**Fig 2E** shows one hemisphere of one animal, but results were very
189 similar in other hemispheres of other animals, see **Fig S1**). We show separate maps for each of
190 the different sets of statistics used to constrain the synthetic sounds (cochlear, temporal
191 modulation, spectral modulation and spectrotemporal modulation). Below we plot corresponding
192 maps from humans. The human maps are based on data averaged across subjects, but similar
193 results were observed in individual subjects (Norman-Haignere and McDermott, 2018).
194

195 In ferrets, we observed a similar pattern throughout both primary and non-primary regions:
196 responses became more similar as we matched additional acoustic features with NSE values
197 close to 0 for sounds matched on the full spectrotemporal model. This pattern contrasts sharply
198 with that observed in humans, where we observed a clear and substantial rise in NSE values
199 when moving from primary to non-primary auditory cortex even for sounds matched on joint
200 spectrotemporal modulations statistics. We quantified these effects by measuring NSE values
201 using ROIs binned based on distance to primary auditory cortex, as was done previously in
202 humans (**Fig 2F**). This analysis revealed a substantial and significant rise in NSEs when matching
203 additional acoustic features in ferrets (NSE spectrotemporal < NSE temporal < NSE spectral <
204 NSE cochlear, $p < 0.01$ via a bootstrapping analysis across the sound set). But there was little
205 difference in NSEs between ferret primary and non-primary regions, with NSE values close to
206 zero in all regions for spectrotemporally matched synthetics. In contrast, every human subject
207 tested showed larger NSE values in non-primary regions, yielding a significant species difference
208 ($p < 0.01$ via a sign-test comparing each ferret to all of the human subjects tested; see Methods
209 for details).
210

211 **Assessing and comparing selectivity for frequency and modulation across species**

212 Our NSE maps suggest that ferret cortical responses are selective for frequency and modulation,
213 but do not reveal how this selectivity is organized or whether it is similar to that in humans. While
214 it is not feasible to inspect or plot all individual voxels, we found that fUS responses like human
215 fMRI responses are low-dimensional and can be explained as the weighted sum of a small number
216 of component response patterns. This observation served as the basis for our denoising

217 procedure, as well as a useful way to examining ferret cortical selectivity and comparing that
 218 selectivity with humans. We found that we could discriminate approximately 8 distinct component
 219 response patterns before over-fitting to noise (**Fig S2C**).



220
 221 **Figure 3: Organization of frequency and modulation selectivity in ferret auditory cortex, revealed by**
 222 **component analysis.** **A**, For reference with the weight maps in panel B, a tonotopic map is shown, measured
 223 using pure tones. The map is from one hemisphere of one animal (Ferret T, left). **B**, Voxel weight maps from
 224 three components, inferred using responses to natural and synthetic sounds (see **Fig S3** for all 8 components
 225 and **Fig S4** for all hemispheres). The maps for components f1 and f2 closely mirrored the high and low-
 226 frequency tonotopic gradients respectively. **C**, Component response to natural and spectrotemporally-
 227 matched synthetic sounds, colored based on category labels (labels shown at the bottom left of the figure).
 228 Components f1 and f2 did not respond selectively to particular categories. Component f3 responded
 229 preferentially to speech sounds. **D**, Correlation of component responses with energy at different audio
 230 frequencies, measured from a cochleagram. Inset for f3 shows the correlation pattern that would be expected
 231 from a response that was perfectly selective for speech (i.e. 1 for speech, 0 for all other sounds). **E**,
 232 Correlations with modulation energy at different temporal and spectral rates. Inset shows the correlation
 233 pattern that would be expected for a perfectly speech-selective response.

234
 235 We first examined the selectivity of the inferred response patterns and their anatomical distribution
 236 of weights in the brain (**Fig 3** shows three example components; **Fig S3** shows all 8 components).
 237 All of the component response profiles showed significant correlations with measures of energy
 238 at different cochlear frequencies and spectrotemporal modulation rates (**Fig 3D-E**) ($p < 0.01$ for
 239 all components for both frequency and modulation features; statistics computed via a permutation
 240 test across the sound set). Two components (f1 & f2) had responses that correlated with energy
 241 at high and low-frequencies respectively, with voxel weights that mirrored the tonotopic gradients
 242 measured in these animals (compare **Fig 3B** and **3A**; see **Fig S4** for all hemispheres/animals),
 243 similar to the tonotopic components previously identified in humans (Norman-Haignere et al.,
 244 2015) (**Fig S5**, components h1 and h2). We also observed components with weak frequency
 245 tuning but prominent tuning for spectrotemporal modulations (**Fig S3**), again similar to humans.
 246 Surprisingly, one component (f3) responded selectively to speech sounds, and its response
 247 correlated with energy at frequency and modulation rates characteristic of speech (insets in **Fig**
 248 **3D-E**, bottom row). But notably, all of the inferred components, including the speech-selective
 249 component, produced very similar responses to natural and synthetic sounds (**Fig 3C**), suggesting

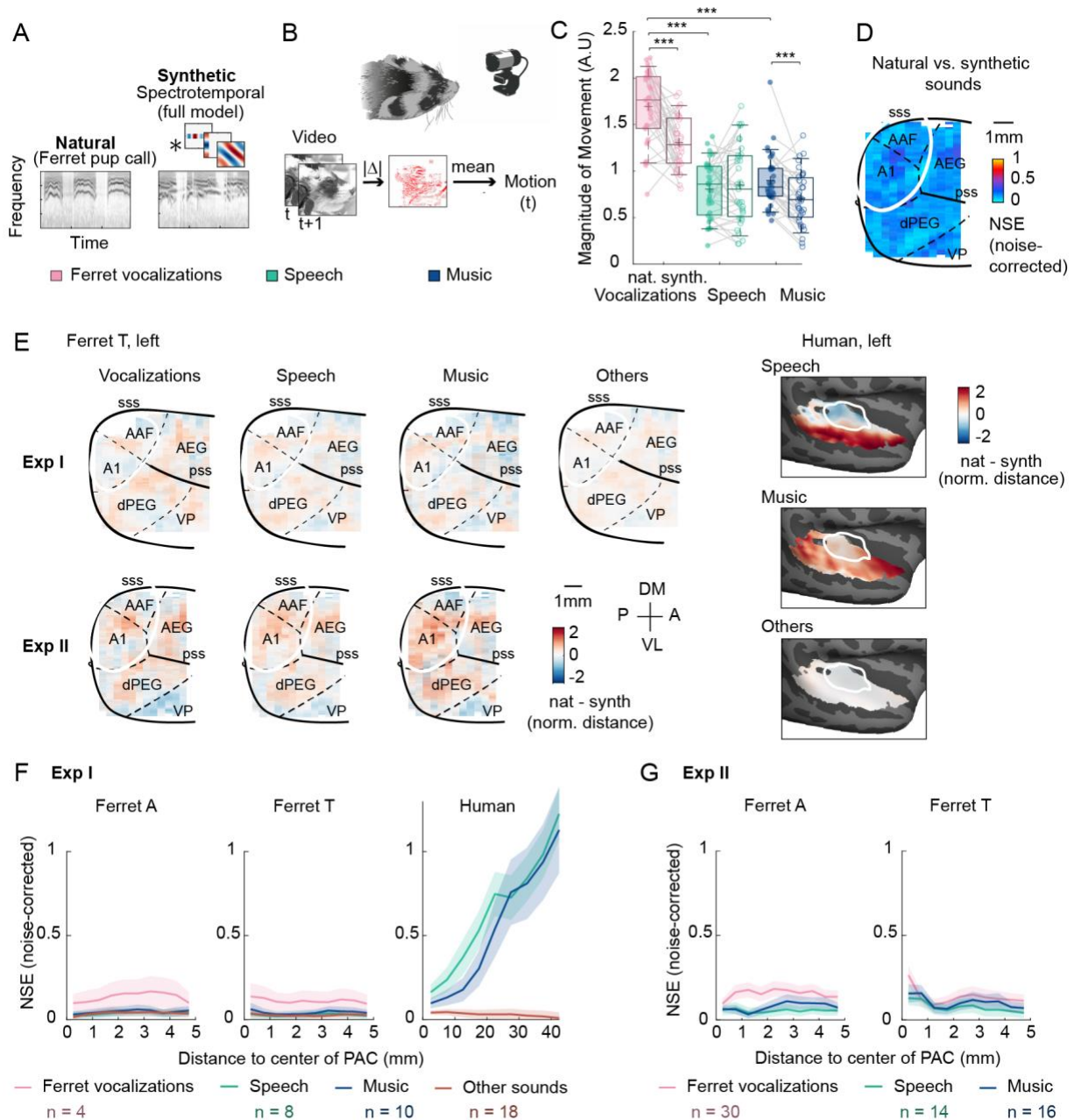
250 that their selectivity can be explained by their tuning for frequency and modulation. This contrasts
251 with the speech- and music-selective components previously observed in humans, which
252 responded selectively to natural speech and music, respectively, and which clustered in distinct
253 non-primary regions of human auditory cortex (see **Fig S5**, components h5 and h6).
254

255 The frequency and modulation selectivity evident in the ferret components appeared similar to
256 that in humans (Norman-Haignere et al., 2015). To quantitatively evaluate similarity, we attempted
257 to predict the response of each human component, inferred from our prior work, from those in the
258 ferrets (**Fig S6**) and vice versa (**Fig S7**). We found that much of the component response variation
259 to synthetic sounds could be predicted across species (**Fig S6B&D, S7A&C**). This finding is
260 consistent with the hypothesis that tuning for frequency and modulation is similar across species,
261 since the synthetic sounds only varied in their frequency and modulation statistics. In contrast,
262 differences between natural vs. synthetic sounds were only robust in humans and as a
263 consequence could not be predicted from responses in ferrets (**Fig S6C&E**). Thus, selectivity for
264 frequency and modulation is both qualitatively and quantitatively similar across species, despite
265 large and substantial differences in higher-order tuning.
266

267 **Experiment II: Testing the importance of ecological relevance**

268 Experiment I included more speech (8) and music (10) sounds than ferret vocalizations (4). We
269 have previously found that differences between natural and synthetic sounds in humans are
270 mostly driven by speech and music (Norman-Haignere and McDermott, 2018), which could be
271 due to their more complex structure (McDermott and Simoncelli, 2011), their ecological relevance,
272 or a combination of the two. Given this fact, it seemed possible that the observed species
273 difference might reflect a difference in the ecological relevance of the natural sounds tested. To
274 test this possibility, we performed a second experiment that included many more ferret
275 vocalizations (30) (**Fig 4A**), as well as a smaller number of speech (14) and music (16) sounds to
276 allow comparison with Experiment I. We only synthesized sounds matched in their full
277 spectrotemporal modulation statistics to be able to test a broader sound set.
278

279 Using a video recording of the animals' face (**Fig 4B**), we found that the ferrets showed greater
280 spontaneous movements during the presentation of the natural ferret vocalizations compared with
281 both the synthetic sounds and the other natural sounds (**Fig 4C**; see **Fig S8** for additional plots
282 from individual animals and finer-grained vocalization categories). This observation demonstrates
283 that natural ferret vocalizations contain additional structure that is missing from their synthetic
284 counterparts, and that this additional structure is sufficiently salient to cause a spontaneous
285 increase in motion without any overt training. Moreover, the behavioral differences between
286 natural and synthetic vocalizations were greater than those for speech ($p < 0.001$ via Wilcoxon
287 signed-rank test) and music ($p < 0.05$), consistent with their greater ecological relevance. To
288 prevent motion from affecting the ultrasound responses, we designed a denoising procedure that
289 greatly minimized correlations between the ultrasound responses and motion without removing
290 sound-evoked activity (see Methods and Appendix).



291
 292 **Figure 4. Testing the importance of ecological relevance.** **A**, Experiment II measured responses to a
 293 much larger number of ferret vocalizations (30), as well as a smaller number of speech (14) and
 294 music (16) sounds, unlike Experiment I which only tested 4 ferret vocalizations. Cochleograms for an example natural
 295 and synthetic vocalization (a “pup call”) are plotted. **B**, The animal’s spontaneous movements were monitored
 296 with a video recording of the animal’s face. Motion was measured as the mean absolute deviation between
 297 adjacent video frames, averaged across pixels. **C**, Average evoked movement amplitude for natural (shaded)
 298 and synthetic (unshaded) sounds broken down by category. Each dot represents one recording session.
 299 Significant differences between natural and synthetic sounds, and between categories of natural sounds
 300 are plotted (paired Wilcoxon test, $p < 0.001$: ***). Evoked movement amplitude was normalized by the standard
 301 deviation across sounds for each recording session prior to averaging across sound category (necessary
 302 because absolute pixel deviations cannot be meaningfully compared across sessions). Results were
 303 consistent across ferrets (**Fig S8A**). Both animals moved substantially more during natural ferret vocalizations
 304 compared with both matched synthetics as well as speech and music. **D**, Map showing the dissimilarity
 305 between natural and spectrotemporally matched synthetic sounds from Experiment II for one hemisphere
 306 (Ferret T, left; see **Fig S8B** for all hemispheres), measured using the noise-corrected NSE across sounds.
 307 NSE values were low across auditory cortex, replicating the first experiment. **E**, Maps showing the average
 308 difference between responses to natural and synthetic sounds for vocalizations, speech, music, and others
 309 sounds, normalized for each voxel by the standard deviation across all sounds. Results are shown for the

310 same ferret hemisphere (T, left) for both Experiment I and II. Humans were only tested in Experiment I. **F**,
311 NSE for different sound categories, plotted as a function of distance to primary auditory cortex (binned as in
312 **Fig 2F**). Shaded area represents ± 1 s.e.m. (**Fig S8D** plots NSEs for individual sounds) **G**, Same as panel
313 **F** but showing results from Experiment II.

314
315 Despite this clear behavioral difference, we nonetheless found that voxel responses to natural
316 and synthetic sounds were similar throughout primary and non-primary regions, yielding small
317 NSE values (**Fig 4D**). This result demonstrates that our key findings from Experiment I are not
318 due to the weak ecological relevance of the tested sounds, since a qualitatively similar result was
319 obtained in Experiment II when half of the sounds were ferret vocalizations.

320
321 To directly test if ferrets showed selective responses to natural vs. synthetic ferret vocalizations,
322 we computed maps showing the average difference between natural vs. synthetic sounds for
323 different categories, using data from both Experiments I and II (**Fig 4E**). We also separately
324 measured the NSE for sounds from different categories (**Fig 4F-G**; note the normalization term in
325 the NSE was computed using all sounds to avoid inadvertently normalizing out meaningful
326 differences between sounds/categories). We plot the median NSE for sounds from different
327 categories as a function of distance to primary auditory cortex for each animal and experiment
328 (**Fig 4F-G**; **Fig S8D-E** shows the distribution of NSE values for individual sound pairs). This
329 analysis revealed that NSE values in ferrets were slightly elevated for ferret vocalizations
330 compared with other categories (**Fig 4F-G**), consistent with their ecological relevance. This effect,
331 however, was small and inconsistent, reaching significance in only one of the two animals in
332 Experiment II (Ferret A, $p < 0.005$, Wilcoxon test) (the effect was significant in both animals in
333 Experiment I, but this experiment only tested 4 ferret vocalizations). Moreover, the small
334 differences that were present between natural and synthetic sounds were spatially distributed
335 throughout primary and non-primary regions, and very similar to those for speech, music and
336 other natural sounds (**Fig 4E**). In contrast, humans showed large and selective responses to
337 speech and music that were concentrated in distinct non-primary regions (lateral for speech and
338 anterior/posterior for music) and clearly different from those for other natural sounds (**Fig 4E**).
339 Thus, ferrets do not show any of the neural signatures of higher-order selectivity that we previously
340 identified in humans (large effect size, spatially clustered responses, and a clear non-primary
341 bias), even for con-specific vocalizations, which produced clear behavioral differences reflecting
342 their ecological significance.

343 344 **Discussion**

345
346 Our study reveals a prominent divergence in the representation of ecologically relevant natural
347 sounds between humans and ferrets. Using a recently developed wide-field imaging technique
348 (functional Ultrasound), we measured cortical responses in the ferret to a set of natural and
349 spectrotemporally-matched synthetic sounds previously tested in humans. We found that
350 selectivity for frequency and modulation statistics in the synthetic sounds was similar across
351 species. But unlike humans, who showed selective responses to natural speech and music in
352 non-primary auditory cortex, ferrets cortical responses to natural and synthetic sounds were
353 similar throughout primary and non-primary regions, even when tested with ferret vocalizations.
354 This finding suggests that speech and music have substantially altered higher-order acoustic
355 representations in human auditory cortex, but have largely preserved tuning for lower-level
356 acoustic features like frequency and spectrotemporal modulation.

357 358 ***Species differences in the representation of natural sounds***

359 The central challenge of sensory coding is that behaviorally relevant information is often not
360 explicit in the inputs to sensory systems. As a consequence, sensory systems transform their
361 inputs into higher-order representations that expose behaviorally relevant properties of stimuli

362 (DiCarlo and Cox, 2007; Mizrahi et al., 2014; Theunissen and Elie, 2014). The early stages of this
363 transformation are thought to be conserved across many species. For example, all mammals
364 transduce sound pressure waveforms into a frequency-specific representation of sound energy in
365 the cochlea, although the resolution and frequency range of cochlear tuning differ across species
366 (Bruns and Schmieszek, 1980; Köppl et al., 1993; Joris et al., 2011; Walker et al., 2019). But it
367 has remained unclear whether representations at later stages are similarly conserved across
368 species.

369
370 Only a few studies have attempted to compare cortical representations of natural stimuli between
371 humans and other animals, and these studies have typically found similar representations in
372 auditory cortex. Studies of speech phonemes in ferrets (Mesgarani et al., 2008) and macaques
373 (Steinschneider et al., 2013) have replicated many neural phenomena observed in humans
374 (Mesgarani et al., 2014). A recent fMRI study found that maps of spectrotemporal modulation
375 tuning, measured using natural sounds, are coarsely similar between humans and macaques,
376 although slow temporal modulations which are prominent in speech were better decoded in
377 humans compared with macaques (Erb et al., 2019), potentially analogous to prior findings of
378 enhanced cochlear frequency tuning for behaviorally relevant sound frequencies (Bruns and
379 Schmieszek, 1980; Köppl et al., 1993). Thus, prior work has revealed quantitative differences in
380 the extent and resolution of neural tuning for different acoustic frequencies and modulation rates.
381 But it has remained unclear whether there are qualitative differences in how natural sounds are
382 represented across species.

383
384 Our study demonstrates that human non-primary regions exhibit a form of higher-order acoustic
385 selectivity that is almost completely absent in ferrets. Ferret cortical responses to natural and
386 spectrotemporally matched synthetic sounds were closely matched throughout their auditory
387 cortex, and the small differences that we observed were scattered throughout primary and non-
388 primary regions (**Fig 4E**), unlike the pattern observed in humans. As a consequence, the
389 differences that we observed between natural and synthetic sounds in humans were not
390 predictable from cortical responses in ferrets (**Fig S6C**), even though we could predict responses
391 to synthetic sounds across species (**Fig S6B&E**). This higher-order selectivity is unlikely to be
392 explained by explicit semantic knowledge about speech or music, since similar responses are
393 observed for foreign speech (Norman-Haignere et al., 2015; Norman-Haignere and McDermott,
394 2018) and music selectivity is robust in listeners without musical training (Boebinger et al., 2020).
395 These results suggest that humans develop or have evolved a higher-order stage of acoustic
396 analysis, potentially specific to speech and music, that cannot be explained by standard frequency
397 and modulation statistics and is largely absent from the ferret brain. This specificity for speech
398 and music could be due to their acoustic complexity, and/or their behavioral relevance, as
399 discussed further below.

400
401 By comparison, our study suggests that there is a substantial amount of cross-species overlap in
402 the cortical representation of frequency and modulation features. Both humans and ferrets
403 exhibited tonotopically organized selectivity for different frequencies. But this frequency selectivity
404 only accounted for a relatively small fraction of the voxel response to natural sounds (**Fig 2E**),
405 even in primary auditory cortex, which emphasizes the importance of modulation tuning in
406 explaining cortical responses in both humans and ferrets. Like humans, ferrets showed spatially
407 organized selectivity for different temporal and spectral modulation rates, that coarsely mimicked
408 the types of selectivity we have previously observed in humans, replicating prior findings (Erb et
409 al., 2019). And this selectivity was sufficiently similar that we could quantitatively predict response
410 patterns to the synthetic sounds across species. These results do not imply that frequency and
411 modulation tuning is identical across species, but do suggest that the organization is qualitatively
412 similar.

413
414 Our results also do not imply that ferrets lack higher-order acoustic representations. Indeed, we
415 found that ferrets' spontaneous movements robustly discriminated between natural and synthetic
416 ferret vocalizations, demonstrating behavioral sensitivity to the features which distinguish these
417 sound sets, and this sensitivity was greater for ferret vocalizations than for either speech or music.
418 But the manner in which species-relevant higher-order features are represented is likely distinct
419 between humans and ferrets. For example, it is also possible that selectivity for higher-order
420 features is more distributed in ferret auditory cortex, which is consistent with our finding that
421 differences between natural and synthetic sounds are weak, distributed throughout primary and
422 non-primary regions, and show a mix of enhanced and suppressive responses (**Fig 4E**), unlike
423 the strong, selective, and localized responses observed in human non-primary regions.

424
425 Our findings are broadly consistent with a recent study that showed differences in responses to
426 simple tone and noise stimuli between humans and macaques (Norman-Haignere et al., 2019).
427 This study found that selective responses to tones vs. noise were substantially larger in human
428 auditory cortex, perhaps due to the importance of speech and music in humans where harmonic
429 structure plays a central role. But the relationship of this finding to the coding of natural sounds
430 remains unclear because the study was mostly limited to simple, artificial stimuli. Our study
431 provides a much broader test of how the encoding of natural sounds differs between humans and
432 ferrets. As a consequence, we were able to identify a substantial divergence in neural
433 representations at a specific point in the cortical hierarchy.

434 435 ***Methodological advances***

436 Our findings were enabled by a recently developed synthesis method, that makes it possible to
437 synthesize sounds with spectrotemporal modulation statistics that are closely matched to those
438 in natural sounds (Norman-Haignere and McDermott, 2018). Because the synthetics are
439 otherwise unconstrained, they lack higher-order acoustic properties present in natural stimuli (e.g.
440 syllabic structure; musical notes, harmonies and rhythms). Comparing neural responses to natural
441 and spectrotemporally-matched synthetic sounds thus provides a way to isolate responses to
442 higher-order properties of natural stimuli that cannot be accounted for by spectrotemporal
443 modulations. This methodological advance was critical to differentiating human and ferret cortical
444 responses. Indeed, when considering natural or synthetic sounds alone, we observed very similar
445 responses between species. We even observed selective responses to speech compared with
446 other natural sounds in the ferret auditory cortex, due to the fact that speech has a unique range
447 of spectrotemporal modulations. Thus, if we had only tested natural sounds, we might have
448 concluded that speech and music-selective responses in the human non-primary auditory cortex
449 reflect the same types of acoustic representations present in ferrets.

450
451 Our study illustrates the utility of wide-field imaging methods in comparing the brain organization
452 of different species (Bimbard et al., 2018; Milham et al., 2018). Most animal physiology studies
453 focus on measuring responses from single neurons or small clusters of neurons in a single brain
454 region. While this approach is clearly essential to understanding the neural code at a fine grain,
455 studying a single brain region can obscure larger-scale trends that are evident across the cortex.
456 Indeed, if we had only measured responses in a single region of auditory cortex, we would have
457 missed the most striking difference between humans and ferrets: the emergence of selective
458 responses to natural sounds in non-primary regions of humans but not ferrets (**Fig 2E**).

459
460 Functional ultrasound imaging provides a powerful way of studying large-scale functional
461 organization in small animals such as ferrets, since it has much better spatial resolution than fMRI
462 (Macé et al., 2011; Bimbard et al., 2018). Because fUS responses are noisy, prior studies,
463 including those from our own lab, have only been able to characterize responses to a single

464 stimulus dimension, such as frequency, typically using a small stimulus set (Gesnik et al., 2017;
465 Bimbard et al., 2018). Here, we developed a denoising method that made it possible to measure
466 highly reliable responses to over a hundred stimuli in a single experiment. We were able to recover
467 at least as many response dimensions as those detectable with fMRI and humans, and those
468 response dimensions exhibited selectivity for a wide range of frequencies and modulation rates.
469 Our study thus pushes the limits of what is possible using ultrasound imaging, and establishes
470 fUS as an ideal method for studying the large-scale functional organization of the animal brain.

471

472 **Assumptions and limitations**

473 The natural and synthetic sounds we tested were closely matched in their time-averaged cochlear
474 frequency and modulation statistics, measured using a standard model of cochlear and cortical
475 modulation tuning (Chi et al., 2005; Norman-Haignere and McDermott, 2018). We focused on
476 time-averaged statistics because fMRI and fUS reflect time-averaged measures of neural activity,
477 due to the temporally slow nature of hemodynamic responses. Thus, a similar response to natural
478 and synthetic sounds indicates that the statistics being matched are sufficient to explain the voxel
479 response. By contrast, a divergent voxel response indicates that the voxel responds to features
480 of sound that are not captured by the model.

481

482 While divergent responses by themselves do not demonstrate a higher-order response, there are
483 several reasons to think that the selectivity we observed in human non-primary regions is due to
484 higher-order tuning for natural sounds. First, the fact that differences between natural and
485 synthetic sounds were much larger in non-primary regions clearly suggests that these differences
486 are driven by higher-order processing above and beyond that present in primary auditory cortex,
487 where spectrotemporal modulations appear to explain much of the voxel response. Second, the
488 natural and synthetic sounds produced by our synthesis procedure are in practice closely matched
489 on a wide variety of spectrotemporal filterbank models (Norman-Haignere and McDermott, 2018).
490 As a consequence, highly divergent responses to natural and synthetic sounds, like those in non-
491 primary auditory cortex, rule out many such models. Third, the fact that responses were
492 consistently stronger for natural vs. synthetic sounds suggests that these non-primary regions
493 respond selectively to features in natural sounds that are not explicitly captured by
494 spectrotemporal modulations and are thus absent from the synthetic sounds.

495

496 As with any study, our conclusions are limited by the precision and coverage of our neural
497 measurements. For example, fine-grained temporal codes, which have been suggested to play
498 an important role in vocalization encoding (Schnupp et al., 2006), cannot be detected with fUS.
499 However, we note that the resolution of fUS is substantially better than fMRI, particularly in the
500 spatial dimension (voxel sizes were more than 1000 times smaller) and thus the species
501 differences we observed are unlikely to be explained by differences in the resolution of fUS vs.
502 fMRI. It is also possible that ferrets might show more prominent differences between natural and
503 synthetic sounds outside of auditory cortex. But even if this were true, it would still demonstrate a
504 clear species difference because humans show robust selectivity for natural sounds in non-
505 primary regions just outside of primary auditory cortex, while ferrets evidently do not.

506

507 ***Possible nature and causes of differences in higher-order selectivity***

508 What features might non-primary human auditory cortex represent, given that spectrotemporal
509 modulations do not explain all of the response? These regions are not highly sensitive to explicit
510 semantic meaning or musical training (Overath et al., 2015; Boebinger et al., 2020), are located
511 just beyond primary auditory cortex, and show evidence of having short integration periods on the
512 scale of hundreds of milliseconds (Overath et al., 2015). Moreover, many of these regions show
513 clear selectivity for speech or music (Leaver and Rauschecker, 2010; Norman-Haignere et al.,
514 2015). This pattern suggests that these regions might exhibit nonlinear tuning for short-term

515 temporal and spectral structure present in speech syllables or musical notes (e.g. harmonic
516 structure, pitch contours, and local periodicity). This hypothesis is consistent with recent work
517 showing sensitivity to phonotactics in non-primary regions of the superior temporal gyrus (Leonard
518 et al., 2015; Brodbeck et al., 2018; Di Liberto et al., 2019), and with a recent study showing that
519 deep neural networks trained to perform challenging speech and music tasks are better able to
520 predict responses in non-primary regions of human auditory cortex (Kell et al., 2018).

521
522 Why might speech and music have preferentially shaped higher-order acoustic representations in
523 the human brain? Synthetic sounds with modulation statistics matched to common environmental
524 sounds often sound perceptually similar to their natural counterparts, in contrast with speech and
525 music where there is a marked perceptual difference (McDermott and Simoncelli, 2011; Norman-
526 Haignere and McDermott, 2018) (listen to examples [here](#)). This fact might explain why the neural
527 differences that we observed between natural and synthetic sounds in humans are mostly limited
528 to speech and music, but could also be due to the unique behavioral significance of speech and
529 music to human hearing. This observation supports the idea that spectrotemporal statistics better
530 capture perceptually relevant information in many environmental sounds. While ferret
531 vocalizations clearly exhibit additional structure not captured by spectrotemporal modulations –
532 since the animals showed clear behavioral sensitivity to the difference between natural vs.
533 synthetic vocalizations – such structure may play a less-essential role in their everyday hearing
534 compared with that present in speech and music in humans. Furthermore, other animals that
535 depend more on higher-order acoustic representations might show more human-like selectivity in
536 non-primary regions. For example, marmosets have a relatively complex vocal repertoire
537 (Agamaite et al., 2015) and depend more heavily on vocalizations than many other species
538 (Eliades and Miller, 2017), and thus might exhibit more prominent selectivity for higher-order
539 properties in their calls. It may also be possible to experimentally enhance selectivity for higher-
540 order properties via extensive exposure and training, particularly at an early age of development
541 (Polley et al., 2006; Srihasam et al., 2014). All of these questions could be addressed in future
542 work using the methods developed here.

543
544
545

546 **Methods**

547

548 **Animal preparation**

549 Experiments were performed in two head-fixed awake ferrets (A and T), across one or both
550 hemispheres (Study 1: A_{left}, A_{right}, T_{left}, T_{right}; Study 2: A_{left}, T_{left}, and T_{right}). Ferret A was a mother
551 (had one litter of pups), while ferret T was a virgin. Experiments were approved by the French
552 Ministry of Agriculture (protocol authorization: 21022) and strictly comply with the European
553 directives on the protection of animals used for scientific purposes (2010/63/EU). Animal
554 preparation and fUS imaging were performed as in Bimbard et al. (2018). Briefly, a metal headpost
555 was surgically implanted on the skull under anaesthesia. After recovery from surgery, a
556 craniotomy was performed over auditory cortex and then sealed with an ultrasound-transparent
557 Polymethylpentene (TPX™) cover, embedded in an implant of dental cement. Animals could then
558 recover for one week, with unrestricted access to food, water and environmental enrichment.
559 Imaging windows were maintained across weeks with appropriate interventions when tissue and
560 bone regrowth were shadowing brain areas of interest.

561

562 **Ultrasound imaging**

563 fUS data are collected as a series of 2D images or ‘slices’. Slices were collected in the coronal
564 plane and were spaced 0.4 mm apart. The slice plane was varied across sessions in order to
565 cover the region-of-interest which included both primary and non-primary regions of auditory
566 cortex. One or two sessions were performed on each day of recording. The resolution of each
567 voxel was 0.1 x 0.1 x ~0.4 mm (the latter dimension, called elevation, being slightly dependent on
568 the depth of the voxel). The overall voxel volume (0.004 mm³) was more than a thousand times
569 smaller than the voxel volume used in our human study (which was either 8 or 17.64 mm³
570 depending on the subjects/paradigm), which helps to account for their smaller brain.

571

572 A separate “Power Doppler” image/slice was acquired every second. Each of these images was
573 computed by first collecting 300 sub-images or ‘frames’ in a short 600 ms time interval (500 Hz
574 sampling rate). Those 300 frames were then filtered to discard global tissue motion from the signal
575 (Demené et al., 2015) (the first 55 principal components were discarded because they mainly
576 reflect motion; see Demené et al., 2015 for details). The blood signal energy also known as Power
577 Doppler was computed for each voxel by summing the squared magnitudes across the 300
578 frames separately for each pixel (Macé et al., 2011). Power Doppler is known to be proportional
579 to blood volume (Macé et al., 2011).

580

581 Each of the 300 frames was itself computed from 11 tilted plane wave emissions (-10° to 10° with
582 2° steps) fired at a pulse repetition frequency of 5500 Hz. Frames were reconstructed from these
583 plane wave emissions using an in-house, GPU-parallelized delay-and-sum beamforming
584 algorithm (Macé et al., 2011).

585

586 **Stimuli for Experiment I**

587 We tested 40 natural sounds: 36 sounds from our prior experiment plus 4 ferret vocalizations (fight
588 call, pup call, fear vocalization, and play call). Each natural sound was 10 seconds in duration.
589 For each natural sound, we synthesized four synthetic sounds, matched on a different set of
590 acoustic statistics of increasing complexity: cochlear, temporal modulation, spectral modulation,
591 and spectrotemporal modulation. The modulation-matched synthetics were also matched in their
592 cochlear statistics to ensure that differences between cochlear and modulation-matched sounds
593 must be due to the addition of modulation statistics. The natural and synthetic sounds were
594 identical to those in our prior paper, except for the four additional ferret vocalizations, which were
595 synthesized using the same algorithm. We briefly review the algorithm below.

596

597 Cochlear statistics were measured from a cochleagram representation of sound, computed by
598 convolving the sound waveform with filters designed to mimic the pseudo-logarithmic frequency
599 resolution of cochlear responses (McDermott and Simoncelli, 2011). The cochleagram for each
600 sound was composed of the compressed envelopes of these filter responses (compression is
601 designed to mimic the effects of cochlear amplification at low sound levels). Modulation statistics
602 were measured from filtered cochleagrams, computed by convolving each cochleagram in time
603 and frequency with a filter designed to highlight modulations at a particular temporal rate and/or
604 spectral scale (Chi et al., 2005). The temporal and spectral modulation filters were only modulated
605 in time or frequency, respectively. There were 9 temporal filters (best rates: 0.5, 1, 2, 4, 8, 16, 32,
606 64, and 128 Hz) and 6 spectral filters (best scales: 0.25, 0.5, 1, 2, 4, 8 cycles per octave).
607 Spectrotemporal filters were created by taking the outer-product of all pairs of temporal and
608 spectral filters in the 2D fourier domain, which results in oriented gabor-like filters.

609
610 Our synthesis algorithm matches time-averaged statistics of the cochleagrams and filtered
611 cochleagrams via a histogram-matching procedure that implicitly matches all time-averaged
612 statistics of the responses (separately for each frequency channel of the cochleagrams and
613 filtered cochleagrams). This choice is motivated by the fact that both fMRI and fUS reflect time-
614 averaged measures of neural activity, because the temporal resolution of hemodynamic changes
615 is much slower than the underlying neuronal activity. As a consequence, if the fMRI or fUS
616 response is driven by a particular set of acoustic features, we would expect two sounds with
617 similar time-averaged statistics for those features to yield a similar response. We can therefore
618 think of the natural and synthetic sounds as being matched under a particular model of the fMRI
619 or fUS response (a more formal derivation of this idea is given in Norman-Haignere et al., 2018).

620
621 We note that the filters used to compute the cochleagram were designed to match the frequency
622 resolution of the human cochlea, which is thought to be somewhat finer than the frequency
623 resolution of the ferret cochlea (Walker et al., 2019). In general, synthesizing sounds from broader
624 filters results in synthetics that differ slightly more from the originals. And thus if we had used
625 cochlear filters designed to mimic the frequency tuning of the ferret cochlea, we would expect the
626 cochlear-matched synthetic sounds to differ slightly more from the natural sounds. However, given
627 that we already observed highly divergent responses to natural and cochlear-matched synthetic
628 sounds in both species, it is unlikely that using broader cochlear filters would change our findings.
629 In general, we have found the matching procedure is not highly sensitive to the details of the filters
630 used. For example, we have found that sounds matched on the spectrotemporal filters used here
631 and taken from Chi et al. (2005), are also well matched on filters with half the bandwidth, with
632 phases that have been randomized, and with completely random filters (Norman-Haignere and
633 McDermott, 2018).

634 635 **Stimuli for Experiment II**

636 Experiment II tested a larger set of 30 ferret vocalizations (5 fight calls, 17 single-pup calls, and 8
637 multi-pup calls where the calls from different pups overlapped in time). The vocalizations
638 consisted of recordings from several labs (our own, Stephen David's and Andrew King's
639 laboratories). For comparison, we also tested 14 speech sounds and 16 music sounds, yielding
640 60 natural sounds in total. For each natural sound, we created a synthetic sound matched on the
641 full spectrotemporal model. We did not synthesize sounds for the sub-models (cochlear, temporal
642 modulation, and spectral modulation), since our goal was to test if there were divergent responses
643 to natural and synthetic ferret vocalizations for spectrotemporally-matched sounds, like those
644 present in human non-primary auditory cortex for speech and music sounds.

645 646 **Procedure for presenting stimuli**

647 Sounds were played through calibrated earphones (Sennheiser IE800 earphones, HDVA 600
648 amplifier, 65 dB) while recording hemodynamic responses via fUS imaging. In our prior fMRI
649 experiments in humans, we had to chop the 10 second stimuli into 2-second excerpts in order to
650 present the sounds in between scan acquisitions, because MRI acquisitions produce a loud sound
651 that would otherwise interfere with hearing the stimuli. Because fUS imaging produces no audible
652 noise, we were able to present the entire 10 second sound without interruption. The experiment
653 was composed of a series of 20-second trials, and fUS acquisitions were synchronized to trial
654 onset. On each trial, a single 10-second sound was played, with 7 seconds of silence before the
655 sound to establish a response baseline, and 3 seconds of post-stimulus silence to allow the
656 response to return to baseline. There was a randomly chosen 3 to 5 second gap between each
657 trial. Sounds were presented in random order, and each sound was repeated 4 times.

658 659 **Mapping of tonotopic organization with pure tones**

660 Tonotopic organization was assessed using previously described methods (Bimbard et al., 2018).
661 In short, responses were measured to 2-second long pure tones from 5 different frequencies (602
662 Hz, 1430 Hz, 3400 Hz, 8087 Hz, 19234 Hz). The tones were played in random order, with 20
663 trials/frequency. Data was denoised using the same method described in *Denoising Part I:
664 Removing components outside of cortex*. Tonotopic maps were created by determining the best
665 frequency of each voxel, defined as the tone evoking the largest Power Doppler signal. We then
666 used these functional landmarks in combination with brain and vascular anatomy to establish the
667 borders between primary and non-primary areas in all hemispheres, as well as to compare them
668 to those obtained with natural sounds (see **Fig S4**).

669 670 **Brain map display**

671 Views from above were obtained by computing the average of the variable of interest in each
672 vertical column of voxels from the upper part of the manually defined cortical mask.

673 674 **Normalized Squared Error (NSE) maps**

675 Like fMRI, the response timecourse of each fUS voxel shows a gradual build-up of activity after a
676 stimulus, due to the slow and gradual nature of blood flow changes. The shape of this response
677 timecourse is similar across different sounds, but the magnitude varies (**Fig 1C**) (fMRI responses
678 show the same pattern). We therefore measured the response magnitude of each voxel by
679 averaging the response to each sound across time (from 3 to 11 seconds post-stimulus onset),
680 yielding one number per sound. Responses were measured from denoised data. We describe the
681 denoising procedure at the end of the Methods because it is more involved than our other
682 analyses.

683
684 We compared the response magnitude to natural and corresponding synthetic sounds using the
685 normalized squared error (NSE), the same metric used in humans. The NSE takes a value of 0 if
686 the response to natural and synthetic sounds is identical, and 1 if there is no correspondence
687 between responses to natural and synthetic sounds. The NSE is defined as:

$$688$$
$$689 \quad (1) \quad NSE = \frac{\mu([x - y]^2)}{\mu(x^2) + \mu(y^2) - 2\mu(x)\mu(y)}$$

690
691 where x and y are response vectors across the sounds being compared (i.e. natural and
692 synthetic) and $\mu(\cdot)$ indicates the vector mean. We noise-corrected the NSE using the test-retest
693 reliability of the voxel responses (see Norman-Haignere et al., 2018 for details). However, we
694 measured the NSE from denoised data, which was highly reliable, and our correction procedure
695 thus only had a small effect on the resulting values.

696

697 **Annular ROI analyses.**

698 We used the same annular ROI analyses from our prior paper to quantify the change in NSE
699 values (or lack thereof) across the cortex. We binned voxels based on their distance to the center
700 of primary auditory cortex, defined tonotopically. We used smaller bin sizes in ferrets (0.5 mm)
701 than humans (5 mm) due to their smaller brains (results were not sensitive to the choice of bin
702 size). **Figure 2F** plots the median NSE value in each bin, plotted separately for each human
703 subject and for each hemisphere of each ferret. To statistically compare different models (e.g.
704 cochlear vs. spectrotemporal), we averaged the NSE values across all bins and
705 hemispheres/subjects separately for each model, bootstrapped the resulting statistics by
706 resampling across the sound set (1000 times), and counted the fraction of samples that
707 overlapped between models (multiplying by 2 to arrive at a two-sided p-value). To compare
708 species, we measured the slope of the NSE vs. distance curve separately for each
709 hemisphere/animal. We found that the slope in every hemisphere of every ferret was less than
710 the slope of every hemisphere of every human subject, which is significant with a sign test ($p <$
711 0.01 ; for each ferret hemisphere there were 8 human subjects to compare with).

712

713 **Component analyses**

714 To investigate the organization of fUS responses to the sound set, we applied the same voxel
715 decomposition used in our prior work in humans to identify a small number of component response
716 patterns that explained a large fraction of the response variation. Like all factorization methods,
717 each voxel is modeled as the weighted sum of a set of canonical response patterns that are
718 shared across voxels. The decomposition algorithm is similar to standard algorithms for
719 independent component analysis (ICA) in that it identifies components that have a non-Gaussian
720 distribution of weights across voxels by minimizing the entropy of the weights (the Gaussian
721 distribution has the highest entropy of any distribution with fixed variance). This optimization
722 criterion is motivated by the fact that independent variables become more Gaussian when they
723 are linearly mixed, and non-Gaussianity thus provides a statistical signature that can be used to
724 unmix the latent variables. Our algorithm differs from standard algorithms for ICA in that it
725 estimates entropy using a histogram, which is effective if there are many voxels, as is the case
726 with fMRI and fUS (40882 fUS voxels for experiment I, 38366 fUS voxels for experiment II).

727

728 We applied our analyses to the denoised response timecourse of each voxel across all sounds
729 (each column of the data matrix contained the concatenated response timecourse of one voxel
730 across all sounds). Our main analysis was performed on voxels concatenated across both animals
731 tested. The results however were similar when the analysis was performed on data from each
732 animal. The number of components was determined via a cross-validation procedure described
733 in the section on denoising.

734

735 We examined the inferred components by plotting and comparing their response profiles to the
736 natural and synthetic sounds, as well as plotting their anatomical weights in the brain. We also
737 correlated the response profiles across all sounds with measures of cochlear and spectrotemporal
738 modulation energy. Cochlear energy was computed by averaging the cochleagram for each sound
739 across time. Spectrotemporal modulation energy was calculated by measuring the strength of
740 modulations in the filtered cochleagrams (which highlight modulations at a particular temporal rate
741 and/or spectral scale). Modulation strength was computed as the standard deviation across time
742 of each frequency channel of the filtered cochleagram. The channel-specific energies were then
743 averaged across frequency, yielding one number per sound and spectrotemporal modulation rate.

744

745 We used a permutation test across the sound set to assess the significance of correlations with
746 frequency and modulation features. Specifically, we measured the maximum correlation across
747 all frequencies and all modulation rates tested, and we compared these values with those from a

748 null distribution computed by permuting the correspondence across sounds between the features
749 and the component responses (1000 permutations). We counted the fraction of samples that
750 overlapped the null distribution and multiplied by two in order to arrive at a two-sided p-value. For
751 every component, we found that correlations with frequency and modulation features were
752 significant ($p < 0.01$).

753

754 **Predicting human components from ferret responses**

755 To quantify which component response patterns were shared across species, we tried to linearly
756 predict components across species (**Fig S6/S7**). Each component was defined by its average
757 response to the 36 natural and corresponding synthetic sounds, matched on the full
758 spectrotemporal model. We attempted to predict each human component from all of the ferret
759 components and vice versa, using cross-validated ridge regression (9 folds). The ridge parameter
760 was chosen using nested cross-validation within the training set (also 9 folds; testing a wide range
761 from 2^{-100} to 2^{100}). Each fold contained pairs of corresponding natural and synthetic sound, so that
762 there would be no overlap between the train and test sounds.

763

764 For each component, we separately measured how well we could predict the response to
765 synthetic sounds (**Fig S6B/S7A**) – which isolates selectivity for frequency and modulation
766 statistics present in natural sounds – as well as how well we could predict the difference between
767 responses to natural vs. synthetic sounds (**Fig S6C/FigS7B**) – which isolates selectivity for
768 features in natural sounds that are not explained by frequency and modulation statistics. We
769 quantified prediction accuracy using the noise-corrected NSE, and we used $(1 - NSE)^2$ as a
770 measure of explained variance. This choice is motivated by the fact $(1 - NSE)$ is equivalent to the
771 Pearson correlation for signals with equal mean and variance and thus $(1 - NSE)^2$ is analogous
772 to the squared Pearson correlation, which is a standard measure of explained variance.

773

774 We multiplied these explained variance estimates by the total response variance of each
775 component for either synthetic sounds or for the difference between natural and synthetic sounds
776 (**Fig S6D/Fig S7C** shows the total variance alongside the fraction of that total variance explained
777 by the cross-species prediction). We noise-corrected the total variance using the equation below:

778

779

$$780 \quad (2) \quad \frac{\text{var}(r_1 + r_2) - \text{var}(r_1 - r_2)}{4}$$

781

782 where r_1 and r_2 are two independent response measurements. Below we give a brief derivation
783 of this equation, where r_1 and r_2 are expressed as the sum of a shared signal (s) that is repeated
784 across measurements plus independent noise (n_1 and n_2) which is not. This derivation utilizes the
785 fact that the variance of independent signals that are summed or subtracted is equal to the sum
786 of their respective variances.

787

$$788 \quad (3) \quad \frac{\text{var}(r_1 + r_2) - \text{var}(r_1 - r_2)}{4} = \frac{\text{var}([s + n_1] + [s + n_2]) - \text{var}([s + n_1] - [s + n_2])}{4}$$
$$789 \quad = \frac{\text{var}(2s + n_1 + n_2) - \text{var}(n_1 - n_2)}{4}$$
$$790 \quad = \frac{4\text{var}(s)}{4}$$
$$791 \quad = \text{var}(s)$$

792

793 The two independent measurements used for noise correction were derived from different human
794 or ferret subjects. The measurements were computed by attempting to predict group components

795 from each individual subject using the same cross-validated regression procedure described
796 above. The two measurements in ferrets came from the two animals tested (A and T). And the
797 two measurements in humans came from averaging across two non-overlapping sets of subjects
798 (4 in each group; groups chosen to have similar SNR).
799

800 For this analysis, the components were normalized so that the RMS magnitude of their weights
801 was equal. As a consequence, components that explained more response variance also had
802 larger response magnitudes. We also adjusted the total variance across all components to equal
803 1.
804

805 **Comparing the similarity of natural and synthetic sounds from different categories.** We
806 computed maps showing the average difference between natural and synthetic sounds from
807 different categories (**Fig 4E**). So that the scale of the differences could be compared across
808 species, we divided the measured differences by the standard deviation of each voxel's response
809 across all sounds. We also separately measured the NSE for sounds from different categories
810 (**Fig 4F,G**). The normalization term in the NSE equation (denominator of equation 1) was
811 averaged across all sounds in order to ensure that the normalization was the same for all
812 sounds/categories and thus that we were not inadvertently normalizing-away meaningful
813 differences between the sounds/categories.
814

815 **Denosing Part I: Removing components outside of cortex**

816 Ultrasound responses in awake animals are noisy, which has limited its usage to mapping simple
817 stimulus dimensions (e.g. frequency) where a single stimulus can be repeated many times
818 (Bimbard et al., 2018). To overcome this issue, we developed a denoising procedure that
819 substantially increased the reliability of the voxel responses (**Fig S9**). The procedure had two
820 parts. The first part, which is described in this section, removed prominent signals outside of
821 cortex, which are likely to reflect movement or other sources of noise. The second part enhanced
822 reliable signals. Code implementing the denoising procedures will be made available upon
823 publication.
824

825 We separated voxels into those inside and outside of cortex, since responses outside of the cortex
826 by definition do not contain stimulus-driven cortical responses, but do contain sources of noise
827 like motion. We then used canonical correlation analysis (CCA) to find a set of response
828 timecourses that were robustly present both inside and outside of cortex, since such timecourses
829 are both likely to reflect noise and likely to distort the responses-of-interest. We projected-out the
830 top 20 canonical components (CCs) from the data set, which we found scrubbed the data of
831 motion-related signals (**Fig S9A**; motion described below).
832

833 This analysis was complicated by one key fact: the animals reliably moved more during the
834 presentation of some sounds (**Fig 4C**). Thus, noise-induced activity outside-of-cortex is likely to
835 be correlated with sound-driven neural responses inside-of-cortex, and removing CCs will thus
836 remove both noise and genuine sound-driven activity. To overcome this issue, we took advantage
837 of the fact that sound-driven responses will by definition be reliable across repeated presentations
838 of the same sound, while motion-induced activity will vary from trial-to-trial for the same sound.
839 We thus found canonical components where the residual activity after removing trial-averaged
840 responses was shared between responses inside and outside of cortex, and we then removed
841 the contribution of these components from the data. We give a detailed description and motivation
842 of this procedure in the **Appendix**, and show the results of a simple simulation demonstrating its
843 efficacy.
844

845 To assess the effect of this procedure on our fUS data, we measured how well it removed signals
846 that were correlated with motion (**Fig S9A**). Motion was measured using a video recording of the
847 animals' face. We measured the motion energy in the video as the average absolute deviation
848 across adjacent frames, summed across all pixels. We correlated this motion timecourse with the
849 residual timecourse of every voxel after subtracting off trial-averaged activity. **Figure S9A** plots
850 the mean absolute correlation value across voxels as a function of the number of canonical
851 components removed (motion can induce both increased and decreased fUS signal and thus it
852 was necessary to take the absolute value of the correlation before averaging). We found that
853 removing the top 20 CCs substantially reduced motion correlations.

854
855 We also found that removing the top 20 CCs removed the spatial striping in the voxel responses,
856 which is a stereotyped feature of motion due to the interaction between motion and blood vessels.
857 To illustrate this effect, **Figure S9B** shows the average difference between responses to natural
858 vs. synthetic sounds in Experiment II (vocalization experiment). Before denoising, this difference
859 map shows a clear striping pattern likely due to the fact that the animals moved more during the
860 presentation of the natural vs. synthetic sounds. The denoising procedure largely eliminated this
861 striping pattern.

862
863 **Denoising Part II: Enhancing signal using DSS**
864 After removing components likely to be driven by noise, we applied a second procedure designed
865 to enhance reliable components in the data. Our procedure is a variant of a method that is often
866 referred to as “denoising source separation” (DSS) or “joint decorrelation” (de Cheveigné and
867 Parra, 2014). In contrast with principal component analysis (PCA), which finds components that
868 have high variance, DSS emphasizes components that have high variance after applying a
869 “biasing” operation that is designed to enhance some aspect of the data. The procedure begins
870 by whitening the data such that all response dimensions have equal variance, the biasing
871 operation is applied, and PCA is then used to extract the components with highest variance after
872 biasing. In our case, we biased the data to enhance response components that were reliable
873 across stimulus repetitions and across the slices from all animals. We note that unlike fMRI, data
874 from different slices come from different sessions. As a consequence, the noise from different
875 slices will be independent. Thus, any response components that are consistent across slices and
876 animals are likely to reflect true, stimulus-driven responses.

877
878 The input to our analysis was a set of matrices. Each matrix contained data from a single stimulus
879 repetition and slice. Only voxels from inside of cortex were analyzed. Each column of each matrix
880 contained the response timecourse of one voxel to all of the sounds (concatenated), denoised
881 using the procedure described in Part I. The response of each voxel was converted to units of
882 percent signal change (the same units used for fMRI analyses) by subtracting and dividing by the
883 pre-stimulus period (also known as percent Cerebral Blood Volume or %CBV in the fUS literature).

884
885 Our analysis involved five steps:
886
887 1. We whitened each matrix individually.
888
889 2. We averaged the whitened response timecourses across repetitions, thus enhancing
890 responses that are reliable across repetitions.
891
892 3. We concatenated the repetition-averaged matrices for all slices across the voxel dimension,
893 thus boosting signal that is shared across slices and animals.

894

895 4. We extracted the top N principal components (PCs) with the highest variance from the
896 concatenated data matrix. The number of components was selected using cross-validation
897 (described below). Because the matrices for each individual repetition and slice have been
898 whitened, the PCs extracted in this step will *not* reflect the components with highest variance, but
899 will instead reflect the components that are the most reliable across repetitions and across
900 slices/animals. We thus refer to these components as “reliable components” (R).

901
902 5. We then projected the data onto the top N reliable components (R):

903
904 (4)
$$D_{denoised} = RR^+D$$

905
906 where D is the denoised response matrix from Part I.

907
908 We used cross-validation to test the efficacy of this denoising procedure and select the number
909 of components (**Fig S2**).

910
911 The analysis involved the following steps:

912
913 1. We divided the sound set into training (75%) and test (25%) sounds. Each set contained
914 corresponding natural and synthetic sounds so that there would be no overlap between train and
915 test sets. We attempted to balance the train and test sets across categories, such that each split
916 had the same number of sounds from each category.

917
918 2. Using responses to just the train sounds (D_{train}), we computed reliable components (R_{train})
919 using the procedure just described (steps 1-4).

920
921 3. We calculated voxel weights for these components:

922
923 (5)
$$W = R_{train}^+ D_{train}$$

924
925 4. We used this weight matrix, which was derived entirely from train data, to denoise responses
926 to the test sounds:

927
928 (6)
$$D_{test-denoised} = R_{test} W$$

929 (7)
$$R_{test} = D_{test} W^+$$

930
931 To evaluate whether the denoising procedure improved predictions, we measured responses to
932 the test sound set using two independent splits of data (odd or even repetitions). We then
933 correlated the responses across the two splits either before or after denoising.

934
935 **Figure S2A** plots the split-half correlation of each voxel before vs. after denoising for every voxel
936 in cortex (using an 8-component model). For this analysis, we either denoised one split of data
937 (blue dots) or both splits of data (green dots). Denoising one split provides a fairer test of whether
938 the denoising procedure enhances SNR, while denoising both splits demonstrates the overall
939 boost in reliability. We also plot the upper bound on the split-half correlation when denoising one
940 split of data (black line), which is given by the square root of the split-half reliability of the original
941 data. We found that our denoising procedure substantially increased reliability with the denoised-
942 correlations remaining close to the upper bound. When denoising both splits, the split-half
943 correlations were close to 1, indicating a highly reliable response.

944

945 **Figure S2B** plots a map in one animal of the split-half correlations when denoising one split of
946 data along with a map of the upper bound. As is evident, the denoised correlations remain close
947 to the upper bound throughout primary and non-primary auditory cortex.
948
949 **Figure S2C** shows the median split-half correlation across voxels as a function of the number of
950 components. Performance was best using ~8 components in both experiments.
951

952 **References**

- 953
- 954 Agamaite JA, Chang C-J, Osmanski MS, Wang X (2015) A quantitative acoustic analysis of the
955 vocal repertoire of the common marmoset (*Callithrix jacchus*). *The Journal of the Acoustical*
956 *Society of America* 138:2906–2928.
- 957 Belin P, Zatorre RJ, Lafaille P, Ahad P, Pike B (2000) Voice-selective areas in human auditory
958 cortex. *Nature* 403:309–312.
- 959 Bimbard C, Demene C, Girard C, Radtke-Schuller S, Shamma S, Tanter M, Boubenec Y (2018)
960 Multi-scale mapping along the auditory hierarchy using high-resolution functional
961 UltraSound in the awake ferret. *Elife* 7:e35028.
- 962 Boebinger D, Norman-Haignere S, McDermott J, Kanwisher N (2020) Cortical music selectivity
963 does not require musical training. *bioRxiv*.
- 964 Brodbeck C, Hong LE, Simon JZ (2018) Rapid transformation from auditory to linguistic
965 representations of continuous speech. *Current Biology* 28:3976–3983.
- 966 Bruns V, Schmieszek E (1980) Cochlear innervation in the greater horseshoe bat: demonstration
967 of an acoustic fovea. *Hearing research* 3:27–43.
- 968 Chi T, Ru P, Shamma SA (2005) Multiresolution spectrotemporal analysis of complex sounds.
969 *The Journal of the Acoustical Society of America* 118:887–906.
- 970 de Cheveigné A, Di Liberto GM, Arzounian D, Wong DD, Hjortkjær J, Fuglsang S, Parra LC (2019)
971 Multiway canonical correlation analysis of brain data. *NeuroImage* 186:728–740.
- 972 de Cheveigné A, Parra LC (2014) Joint decorrelation, a versatile tool for multichannel data
973 analysis. *Neuroimage* 98:487–505.
- 974 de Heer WA, Huth AG, Griffiths TL, Gallant JL, Theunissen FE (2017) The hierarchical cortical
975 organization of human speech processing. *Journal of Neuroscience*:3267–16.
- 976 Demené C, Deffieux T, Pernot M, Osmanski B-F, Biran V, Gennisson J-L, Sieu L-A, Bergel A,
977 Franqui S, Correas J-M (2015) Spatiotemporal clutter filtering of ultrafast ultrasound data
978 highly increases Doppler and fUltrasound sensitivity. *IEEE transactions on medical*
979 *imaging* 34:2271–2285.
- 980 Di Liberto GM, Wong D, Melnik GA, de Cheveigné A (2019) Low-frequency cortical responses to
981 natural speech reflect probabilistic phonotactics. *Neuroimage* 196:237–247.
- 982 DiCarlo JJ, Cox DD (2007) Untangling invariant object recognition. *Trends in cognitive sciences*
983 11:333–341.
- 984 Ding N, Patel AD, Chen L, Butler H, Luo C, Poeppel D (2017) Temporal modulations in speech
985 and music. *Neuroscience & Biobehavioral Reviews*.
- 986 Eliades SJ, Miller CT (2017) Marmoset vocal communication: behavior and neurobiology.
987 *Developmental neurobiology* 77:286–299.

- 988 Erb J, Armendariz M, De Martino F, Goebel R, Vanduffel W, Formisano E (2019) Homology and
989 specificity of natural sound-encoding in human and monkey auditory cortex. *Cerebral*
990 *Cortex* 29:3636–3650.
- 991 Gesnik M, Blaize K, Deffieux T, Gennisson J-L, Sahel J-A, Fink M, Picaud S, Tanter M (2017) 3D
992 functional ultrasound imaging of the cerebral visual system in rodents. *NeuroImage*
993 149:267–274.
- 994 Hickok G, Poeppel D (2007) The cortical organization of speech processing. *Nature reviews*
995 *neuroscience* 8:393–402.
- 996 Joris PX, Bergevin C, Kalluri R, Mc Laughlin M, Michelet P, van der Heijden M, Shera CA (2011)
997 Frequency selectivity in Old-World monkeys corroborates sharp cochlear tuning in
998 humans. *Proceedings of the National Academy of Sciences* 108:17516–17520.
- 999 Kell AJ, Yamins DL, Shook EN, Norman-Haignere SV, McDermott JH (2018) A task-optimized
1000 neural network replicates human auditory behavior, predicts brain responses, and reveals
1001 a cortical processing hierarchy. *Neuron*.
- 1002 Köppl C, Gleich O, Manley GA (1993) An auditory fovea in the barn owl cochlea. *Journal of*
1003 *Comparative Physiology A* 171:695–704.
- 1004 Leaver AM, Rauschecker JP (2010) Cortical representation of natural complex sounds: effects of
1005 acoustic features and auditory object category. *The Journal of Neuroscience* 30:7604–
1006 7612.
- 1007 Leonard MK, Bouchard KE, Tang C, Chang EF (2015) Dynamic encoding of speech sequence
1008 probability in human temporal cortex. *Journal of Neuroscience* 35:7203–7214.
- 1009 Macé E, Montaldo G, Cohen I, Baulac M, Fink M, Tanter M (2011) Functional ultrasound imaging
1010 of the brain. *Nature methods* 8:662.
- 1011 McDermott JH, Simoncelli EP (2011) Sound texture perception via statistics of the auditory
1012 periphery: evidence from sound synthesis. *Neuron* 71:926–940.
- 1013 Mesgarani N, Cheung C, Johnson K, Chang EF (2014) Phonetic feature encoding in human
1014 superior temporal gyrus. *Science* 343:1006–1010.
- 1015 Mesgarani N, David SV, Fritz JB, Shamma SA (2008) Phoneme representation and classification
1016 in primary auditory cortex. *The Journal of the Acoustical Society of America* 123:899–909.
- 1017 Milham MP, Ai L, Koo B, Xu T, Amiez C, Balezeau F, Baxter MG, Blezer EL, Brochier T, Chen A
1018 (2018) An open resource for non-human primate imaging. *Neuron* 100:61–74.
- 1019 Mizrahi A, Shalev A, Nelken I (2014) Single neuron and population coding of natural sounds in
1020 auditory cortex. *Current opinion in neurobiology* 24:103–110.
- 1021 Moore JM, Woolley SM (2019) Emergent tuning for learned vocalizations in auditory cortex.
1022 *Nature neuroscience* 22:1469–1476.
- 1023 Nelken I, Bizley JK, Nodal FR, Ahmed B, King AJ, Schnupp JW (2008) Responses of auditory
1024 cortex to complex stimuli: functional organization revealed using intrinsic optical signals.
1025 *Journal of neurophysiology* 99:1928–1941.









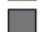

- 1026 Norman-Haignere SV, Kanwisher N, McDermott JH, Conway BR (2019) Divergence in the
1027 functional organization of human and macaque auditory cortex revealed by fMRI responses
1028 to harmonic tones. *Nature Neuroscience* 22:1057.
- 1029 Norman-Haignere SV, Kanwisher NG, McDermott JH (2015) Distinct cortical pathways for music
1030 and speech revealed by hypothesis-free voxel decomposition. *Neuron* 88:1281–1296.
- 1031 Norman-Haignere SV, McDermott JH (2018) Neural responses to natural and model-matched
1032 stimuli reveal distinct computations in primary and nonprimary auditory cortex. *PLoS*
1033 *biology* 16:e2005127.
- 1034 Overath T, McDermott JH, Zarate JM, Poeppel D (2015) The cortical analysis of speech-specific
1035 temporal structure revealed by responses to sound quilts. *Nature neuroscience* 18:903–
1036 911.
- 1037 Patel AD (2012) Language, music, and the brain: a resource-sharing framework. *Language and*
1038 *music as cognitive systems*:204–223.
- 1039 Petkov CI, Kayser C, Steudel T, Whittingstall K, Augath M, Logothetis NK (2008) A voice region
1040 in the monkey brain. *Nature neuroscience* 11:367–374.
- 1041 Polley DB, Steinberg EE, Merzenich MM (2006) Perceptual Learning Directs Auditory Cortical
1042 Map Reorganization through Top-Down Influences. *J Neurosci* 26:4970–4982.
- 1043 Schnupp JW, Hall TM, Kokelaar RF, Ahmed B (2006) Plasticity of temporal pattern codes for
1044 vocalization stimuli in primary auditory cortex. *Journal of Neuroscience* 26:4785–4795.
- 1045 Singh NC, Theunissen FE (2003) Modulation spectra of natural sounds and ethological theories
1046 of auditory processing. *The Journal of the Acoustical Society of America* 114:3394–3411.
- 1047 Srihasam K, Vincent JL, Livingstone MS (2014) Novel domain formation reveals proto-
1048 architecture in inferotemporal cortex. *Nature neuroscience* 17:1776.
- 1049 Steinschneider M, Nourski KV, Fishman YI (2013) Representation of speech in human auditory
1050 cortex: is it special? *Hearing research* 305:57–73.
- 1051 Theunissen FE, Elie JE (2014) Neural processing of natural sounds. *Nature Reviews*
1052 *Neuroscience* 15:355–366.
- 1053 Walker KM, Gonzalez R, Kang JZ, McDermott JH, King AJ (2019) Across-species differences in
1054 pitch perception are consistent with differences in cochlear filtering. *eLife* 8:e41626.
- 1055 Zatorre RJ, Belin P, Penhune VB (2002) Structure and function of auditory cortex: music and
1056 speech. *Trends in Cognitive Sciences* 6:37–46.
- 1057

Experiment I

1. Woman speaking
2. Man speaking
3. Spanish
4. French
5. Italian
6. German
7. Hindi
8. Russian
9. Big band music
10. Bluegrass
11. Cello
12. Orchestra
13. Piano
14. Saxophone
15. Violin
16. Latin music
17. Country song
18. R&B song
19. Biting & chewing
20. Finger tapping

21. Walking on leaves
22. Scratching
23. Walking in heels
24. Writing on paper
25. Heart beat
26. Cicadas
27. Crickets
28. Baby Crying
29. Breathing
30. Clock ticking
31. Siren
32. Keyboard Typing
33. Chimes
34. Chopping food
35. Crumpling paper
36. Keys jingling
37. Ferret fight call
38. Ferret pup call
39. Ferret fear vocalization
40. Ferret play call

Category labels






- | | | |
|---|----------------------|----------------------|
|  | English speech | Speech |
|  | Non-english speech | |
|  | Instrumental music | Music |
|  | Vocal music | |
|  | Human nonvocal | Other sounds |
|  | Animal nonvocal | |
|  | Non-speech vocal | |
|  | Mechanical | |
|  | Environmental | Ferret vocalizations |
|  | Ferret vocalizations | |

Experiment II

1. Spanish
2. French
3. Italian
4. German
5. Hindi
6. Russian
7. English 1
- ...
14. English 7
15. Rock and Roll (50's)
16. Rock and Roll (60's)
17. Classical organ
18. Classical symphony
19. Disco
20. African drumming
21. Funk
22. Jazz

23. Salsa
24. Musical
25. Pop
26. Progressive rock
27. Reggae
28. Epic music
29. R&B song
30. Techno
31. Ferret fight call 1
- ...
35. Ferret fight call 5
36. Single pup call 1
- ...
51. Single pup call 17
52. Multiple pup call 1
- ...
60. Multiple pup call 8

Category labels

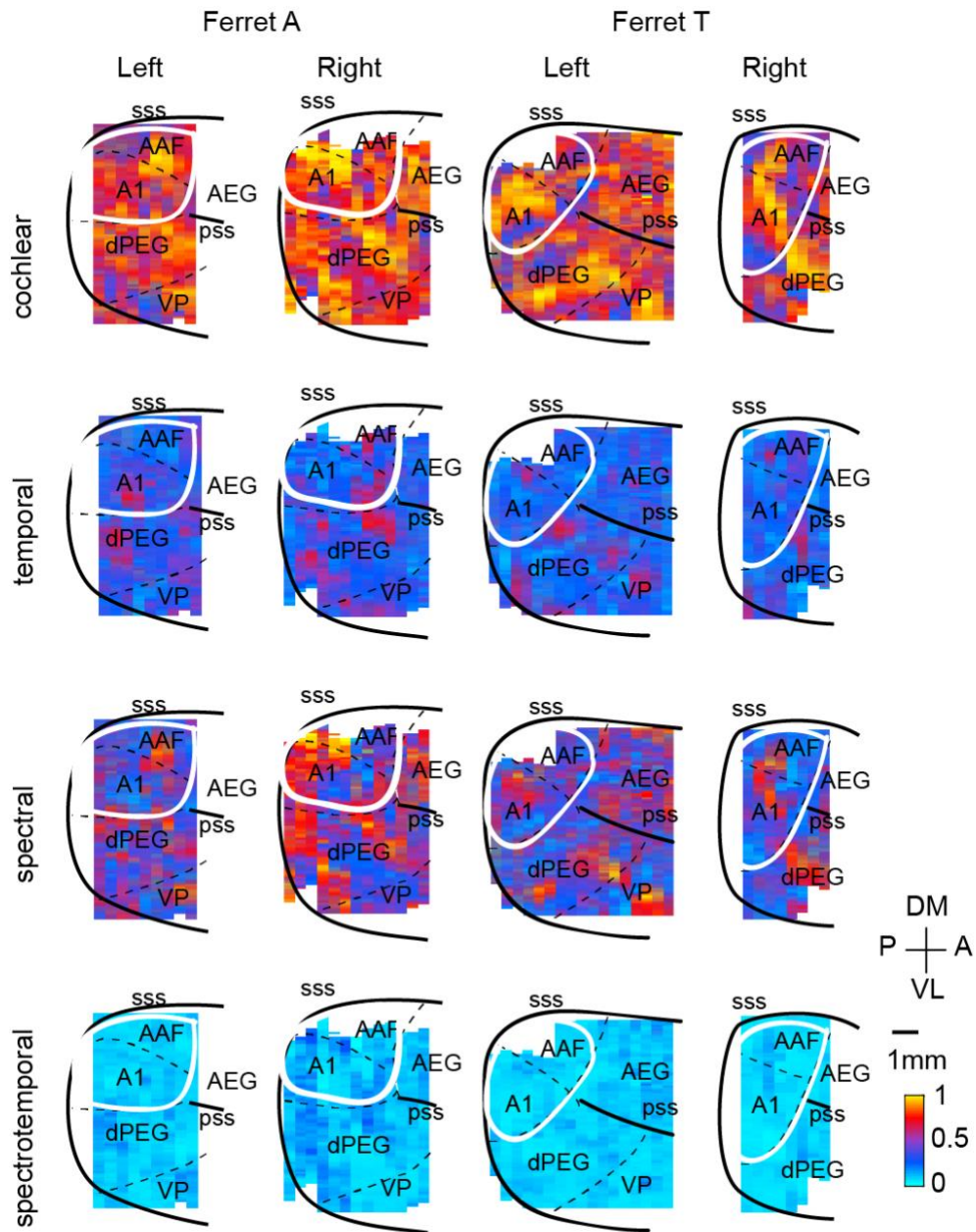
- | | | |
|---|--------------------|----------------------|
|  | Speech | Speech |
|  | Music | |
|  | Ferret fight calls | Ferret vocalizations |
|  | Single pup calls | |
|  | Multiple pup calls | |

1058
1059
1060
1061

Table S1: List of sounds used in both experiments.

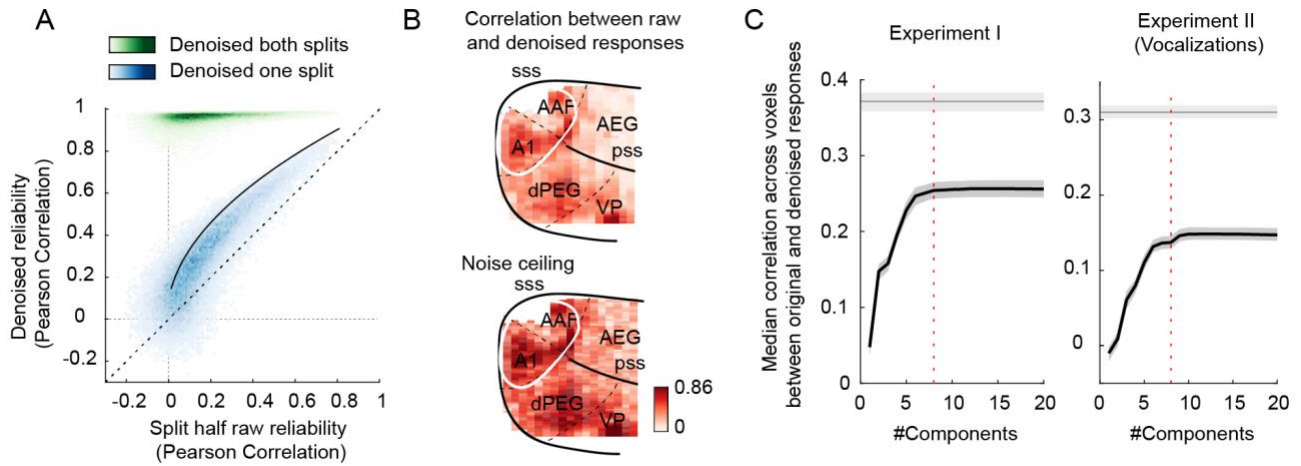
Names of sounds used in Experiments I and II, grouped by category at both fine and coarse scales.

1062
1063



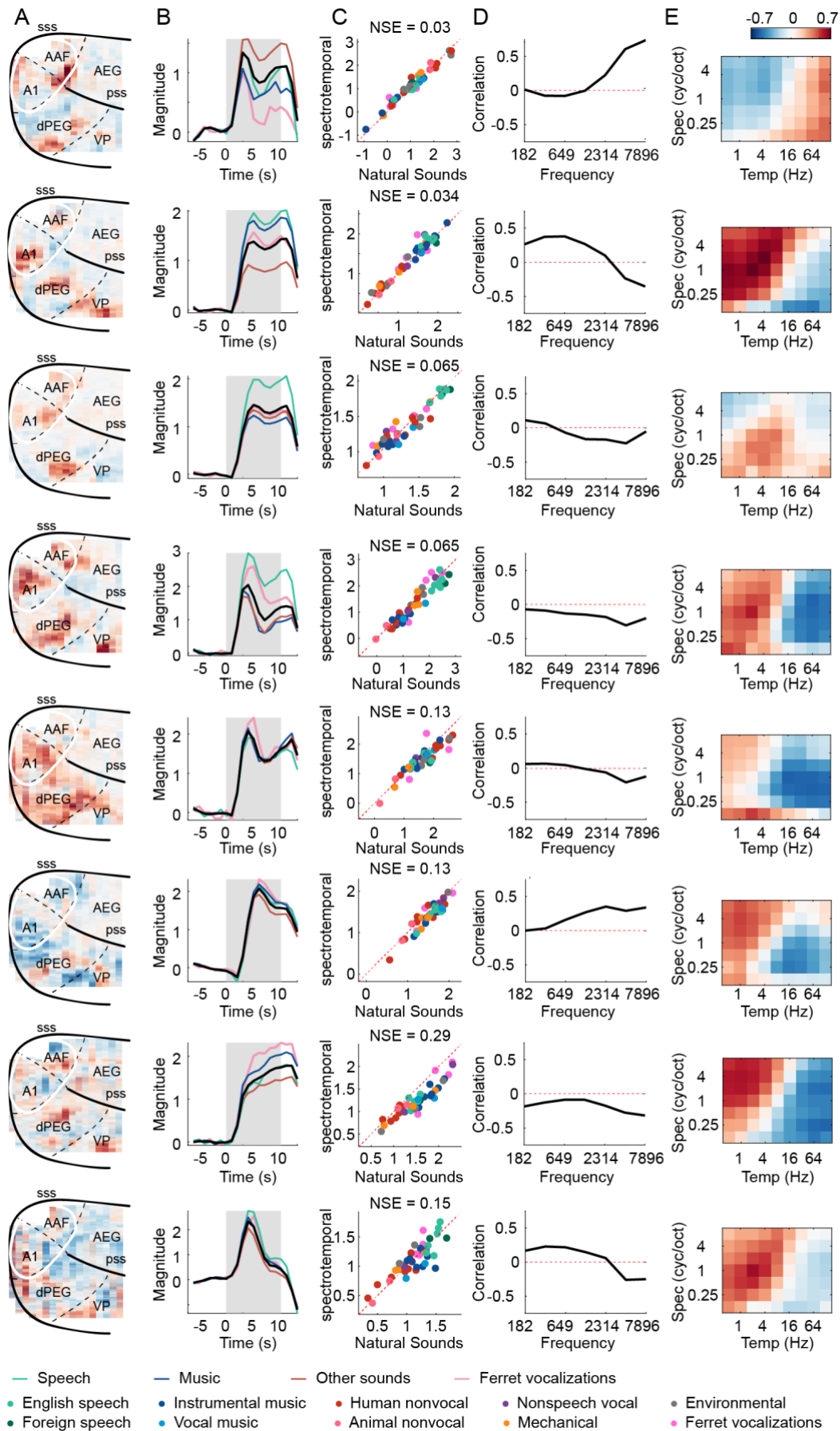
1064
1065

Figure S1. Dissimilarity maps for all hemispheres and animals. Same format as Figure 2E.



1066
1067
1068 **Figure S2. The effect of enhancing reliable signal using a procedure similar to “DSS”** (see
1069 Denoising Part II in Methods) (de Cheveigné and Parra, 2014). **A**, Voxel responses were denoised
1070 by projecting their timecourse onto components that were reliably present across repetitions,
1071 slices and animals. This figure plots the test-retest correlation across independent splits of data
1072 before (x-axis) and after (y-axis) denoising (data from Experiment I). Each dot corresponds to a
1073 single voxel. We denoised either one split of data (blue dots) or both splits of data (green dots).
1074 Denoising one split provides a fairer test of whether the denoising procedure enhances SNR.
1075 Denoising both splits shows the overall effect on response reliability. The theoretical upper-bound
1076 for denoising one split of data is shown by the black line. The denoising procedure substantially
1077 increased data reliability, with the one-split correlations hugging the upper-bound. This plot shows
1078 results from an 8-component model. **B**, This figure plots split-half correlations for denoised data
1079 (one split) as a map (upper panel), along with a map showing the upper bound (right). Denoised
1080 correlations were close to their upper bound throughout auditory cortex. **C**, This figure plots the
1081 median denoised correlation across voxels (one split) as a function of the number of components
1082 used in the denoising procedure. Gray line plots the upper bound. Shaded areas correspond to
1083 95% confidence interval, computed via bootstrapping across the sound set. Results are shown
1084 for both Experiments I (left) and II (right). Predictions were near their maximum using ~8
components in both experiments (the 8-component mark is shown by the vertical dashed line).

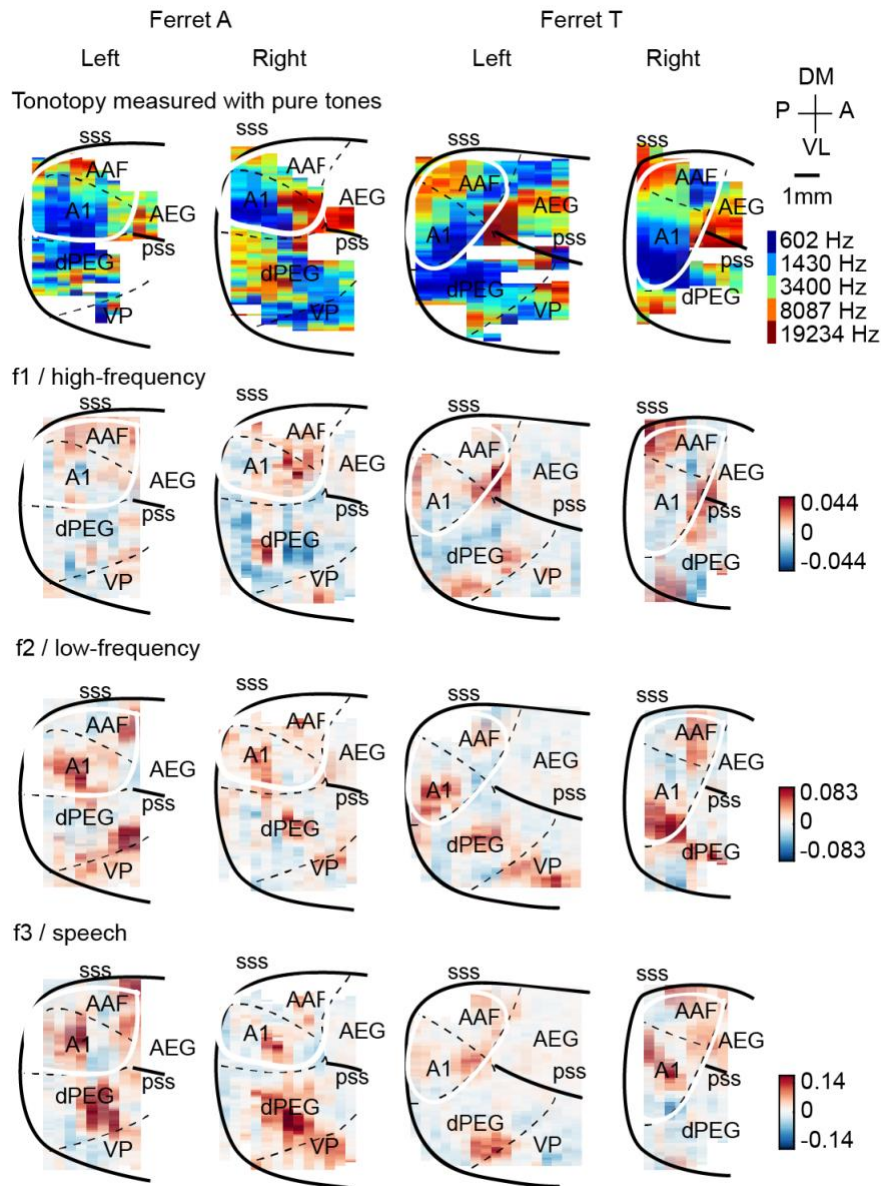
1085



1086

1087 **Figure S3. Results from all 8 ferret components.** Same format as **Figure 3**, except for panel
1088 **B**, which plots the temporal response of the components. Black line shows the average across all
1089 natural sounds. Colored lines correspond to major categories (see **Table S1**): speech (green),
1090 music (blue), vocalizations (pink) and other sounds (brown). Note that the temporal shape varies
1091 across components, but is very similar across sounds/categories within a component, which is
1092 why we summarized component responses by their time-averaged response to each sound.

1093



1094

1095

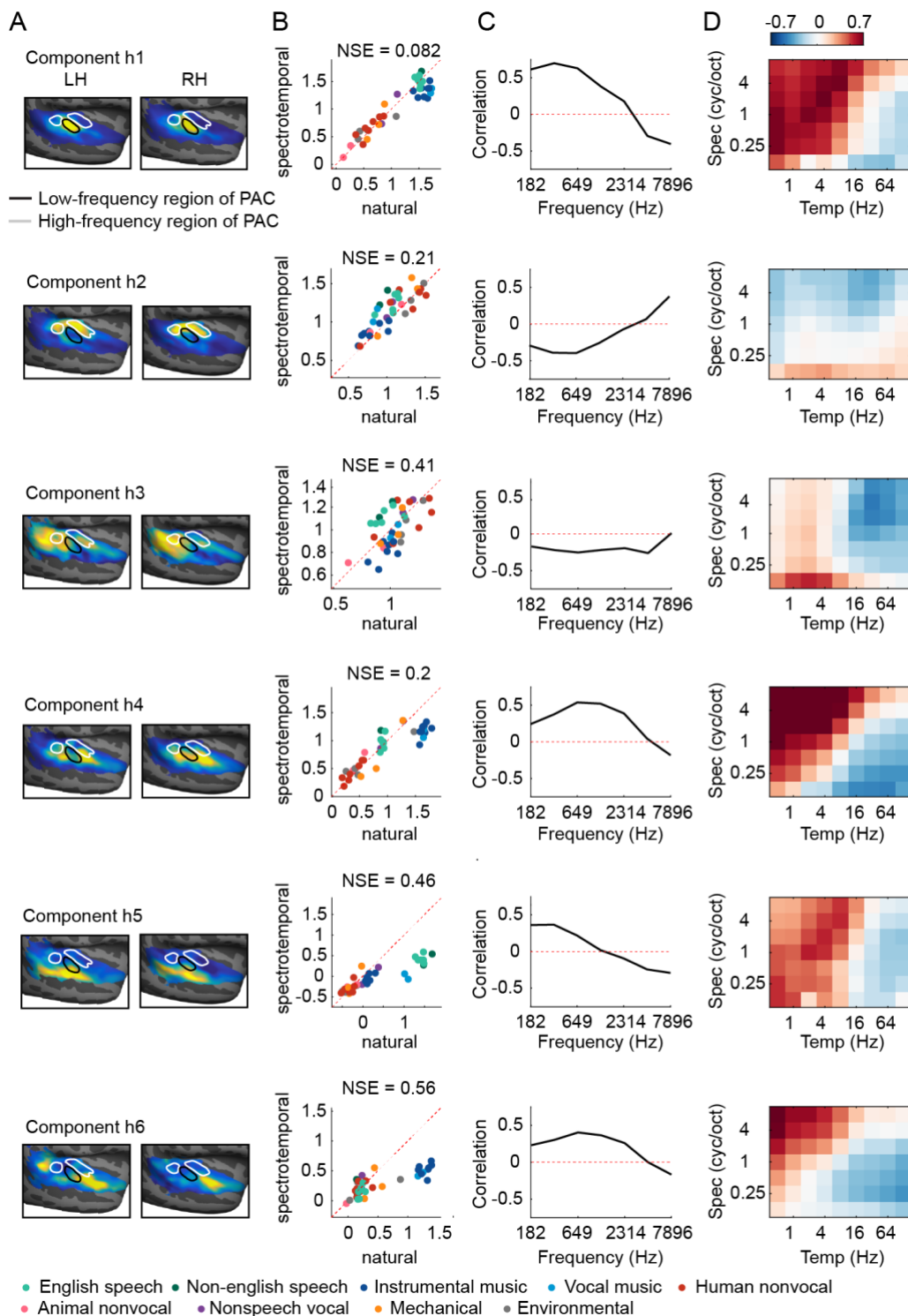
1096

1097

1098

Figure S4. Component weight maps from all hemispheres and ferrets. Weight maps are plotted for the same three components shown in **Figure 3**, but showing maps from all hemispheres of all ferrets tested. For reference, tonotopic maps measured with pure tones are also displayed for the corresponding hemispheres (top row).

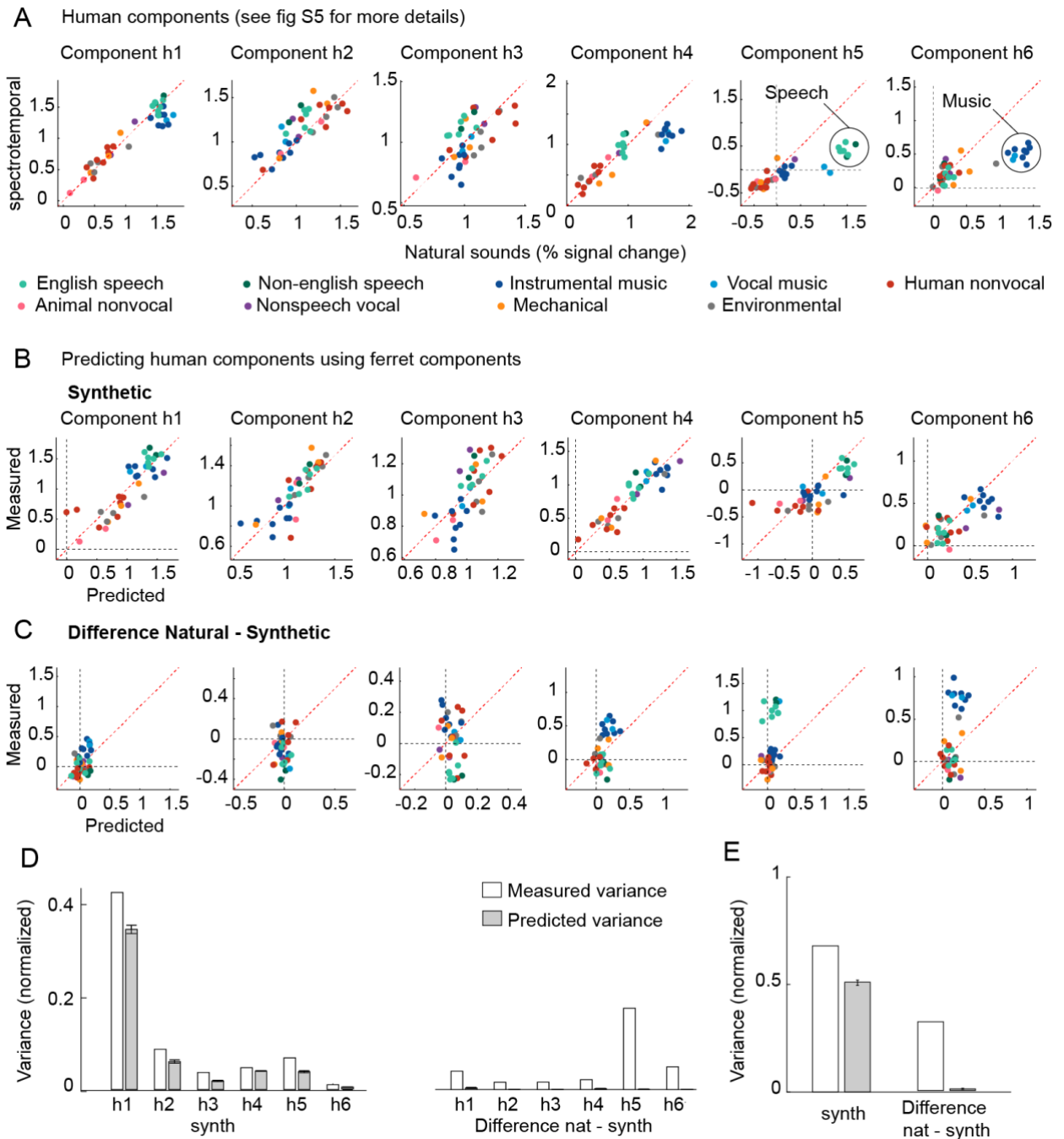
1099
1100



1101
1102
1103
1104
1105

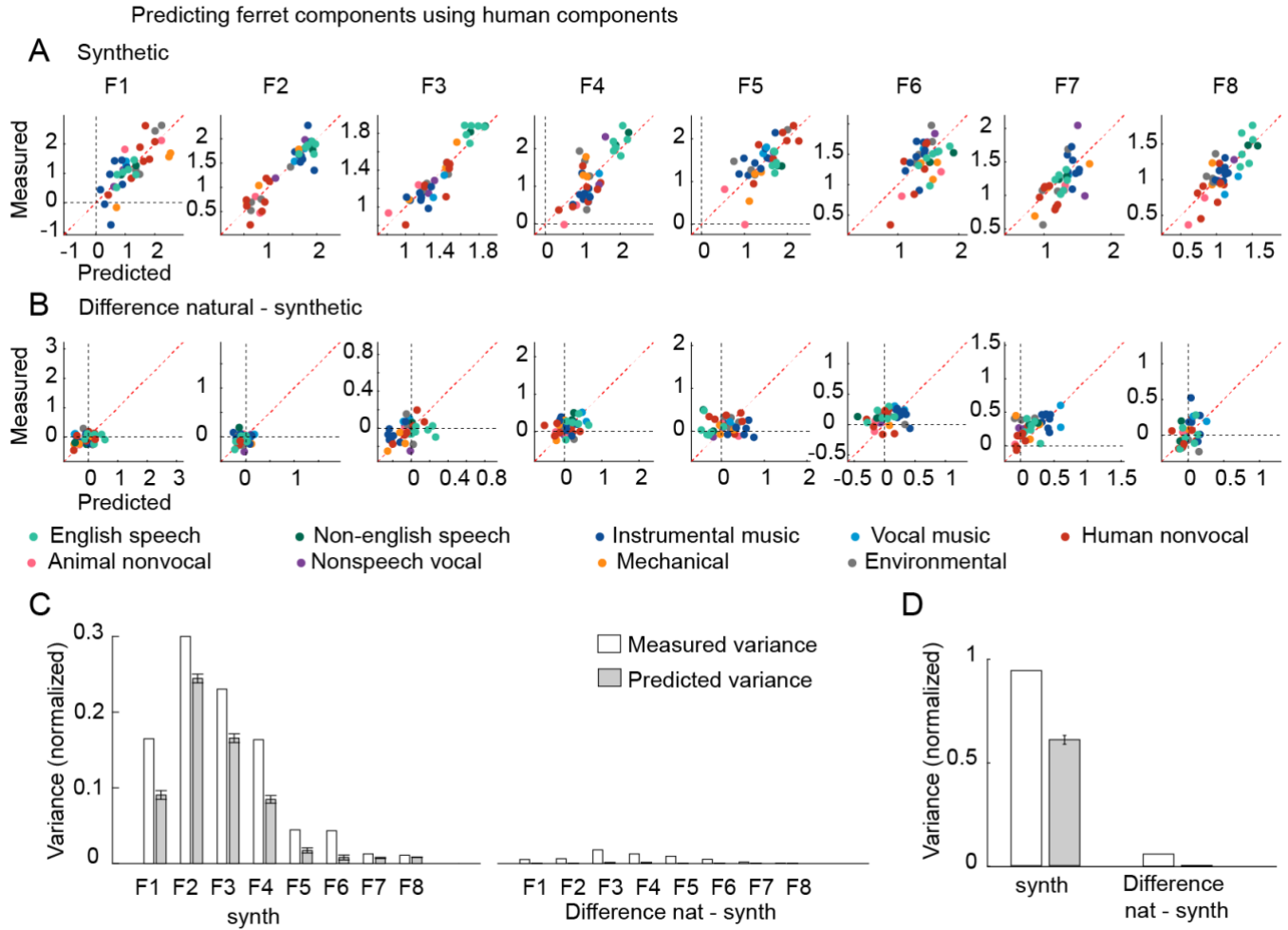
Figure S5. Human components. This figure shows the anatomy and response properties of the six human components inferred in prior work (Norman-Haignere et al., 2015; Norman-Haignere and McDermott, 2018). Same format as **Figure 3**, which plots ferret components. Weight maps (panel A) plot group-averaged maps across subjects.

1106



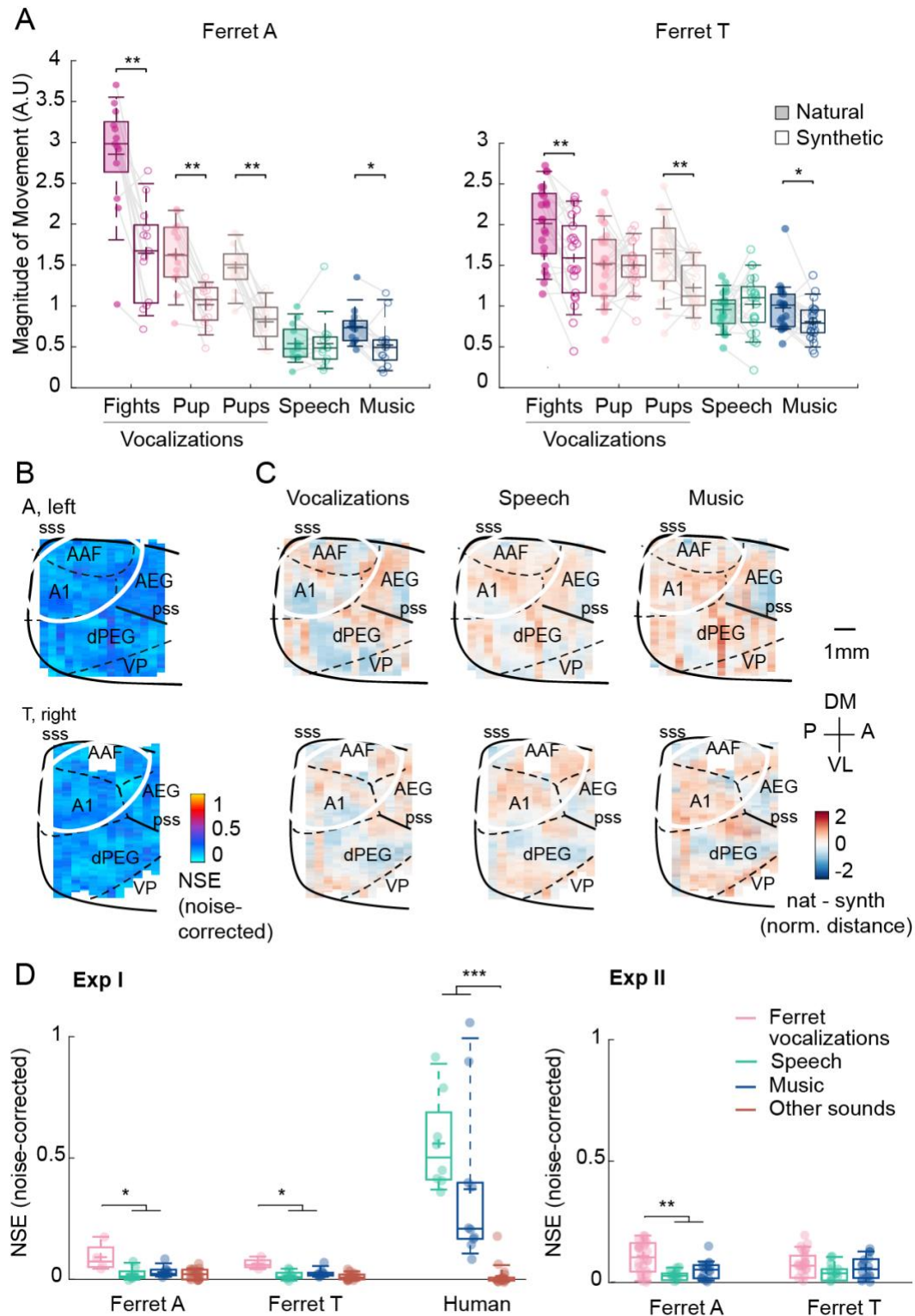
1107
 1108 **Figure S6. Predicting human component responses from ferrets.** This figure plots the results
 1109 of trying to predict the six human components inferred from our prior work (Norman-Haignere et
 1110 al., 2015; Norman-Haignere and McDermott, 2018) from the eight ferret components inferred here
 1111 (see **Fig S7** for the reverse). **A**, For reference, the response of the six human components to
 1112 natural and spectrotemporally matched synthetic sounds is re-plotted here. Components h1-h4
 1113 produced similar responses to natural and synthetic sounds, and had weights that clustered in
 1114 and around primary auditory cortex (**Fig S5**). Components h5 and h6 responded selectively to
 1115 natural speech and natural music, respectively, and had weights that clustered in non-primary
 1116 regions. **B**, This panel plots the measured response of each human component to
 1117 spectrotemporally matched synthetic sounds, along with the predicted response from ferrets. **C**,
 1118 This panel plots the difference between responses to natural and spectrotemporally-matched
 1119 synthetic sounds along with the predicted difference from the ferret components. **D**, Plots the total
 1120 response variance (white bars) of each human component to synthetic sounds (left) and to the

1121 difference between natural and synthetic sounds (right) along with the fraction of that total
1122 response variance predictable from ferrets (gray bars) (all variance measures are noise-
1123 corrected). Error bars show the 95% confidence interval, computed via bootstrapping across the
1124 sound set. **E**, Same as D, but averaged across components.
1125
1126

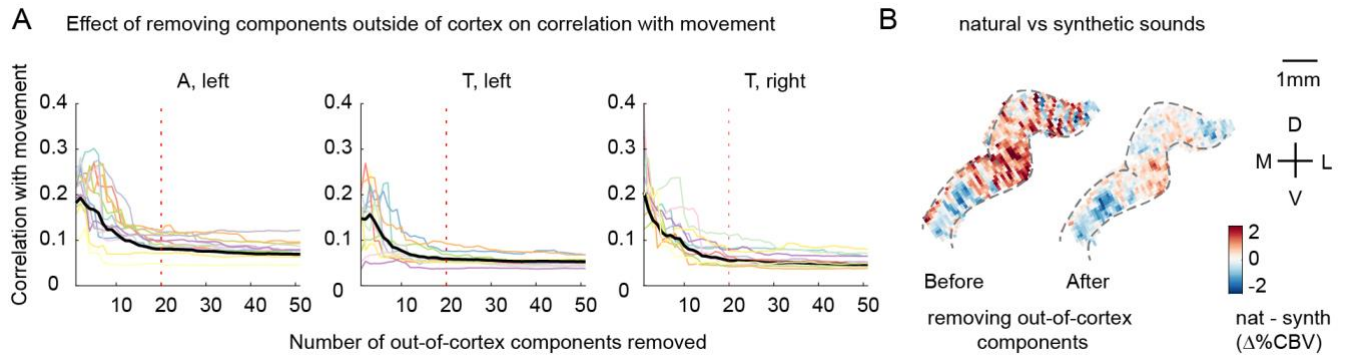


1127
1128
1129
1130

Figure S7. Results of predicting ferret components from human components. Same format as Fig S6B-E.



1131
 1132 **Figure S8. Results of Experiment II from other hemispheres. A-C**, Same format as **Fig 4C-E**,
 1133 except that in panel A the vocalizations are split into sub-categories: fight calls, single pup calls,
 1134 multiple pup calls. Movement amplitude is shown for each animal separately. **D**, This panel shows
 1135 the distribution of NSE values for all pairs of natural and synthetic sounds (median across all
 1136 voxels), grouped by category. The numerator in the NSE calculation is simply the squared error
 1137 for that sound pair, and the denominator is computed in the normal way using responses to all
 1138 sounds (equation 1). Dots show individual sound pairs and box-plots show the median, central
 1139 50% and central 92% (whiskers) of the distribution.



1140

1141

1142

1143

1144

1145

1146

1147

1148

1149

1150

1151

1152

1153

1154

Figure S9. The effect of removing outside-of-cortex components on motion correlations.

Voxel responses were denoised by removing components from outside of cortex, which are likely to reflect artifacts like motion (see Denoising Part I in Methods). **A**, Effect of removing components from outside of cortex on correlations with movement. We measured the correlation of each voxel's response with movement, measured from a video recording of the animal's face (absolute deviation between adjacent frames). Each line shows the average absolute correlation across voxels for a single recording session / slice. Correlation values are plotted as a function of the number of removed components. Motion correlations were substantially reduced by removing the top 20 components (vertical dotted line). **B**, The average difference between responses to natural vs synthetic sounds for an example slice before and after removing the top 20 out-of-cortex components. Motion induces a stereotyped "striping" pattern due to its effect on blood vessels, which is evident in the map computed from raw data, likely because ferrets moved substantially more during natural vs. synthetic sounds (particular for ferret vocalizations; **Figure 4C**). The striping pattern is largely removed by the denoising procedure.

1155 Appendix: Recentered CCA

1156

1157 **Derivation.** The goal of the denoising procedure described in Part I was to remove artifactual
1158 components that were present both inside and outside of cortex, since such components are both
1159 likely to be artifactual and likely to distort the responses-of-interest. The key complication was that
1160 motion-induced artifacts are likely to be correlated with true sound-driven neural activity because
1161 the animals reliably moved more during the presentation of some sounds. To deal with this issue,
1162 we used the fact that motion will vary from trial-to-trial for repeated presentations of the same
1163 sound, while sound-driven responses by definition will not. Here, we give a more formal derivation
1164 of our procedure. We refer to our method as “recentered CCA” (rCCA) for reasons that will
1165 become clear below.

1166

1167 We represent the data for each voxel as an unrolled vector (\mathbf{d}_v) that contains its response
1168 timecourse across all sounds and repetitions. We assume these voxel responses are
1169 contaminated by a set of K artifactual component timecourses $\{\mathbf{a}_k\}$. We thus model each voxel
1170 as a weighted sum of these artifactual components plus a sound-driven response timecourse (\mathbf{s}_v):
1171

$$1172 \quad (8) \quad \mathbf{d}_v = \sum_k^K \mathbf{a}_k w_{k,v} + \mathbf{s}_v$$

1173

1174 Actual voxel responses are also corrupted by voxel-specific noise, which would add an additional
1175 error term to the above equation. In practice, the error term has no effect on our derivation so we
1176 omit it for simplicity (we verified our analysis was robust to voxel-specific noise using simulations,
1177 which are described below).

1178

1179 To denoise our data, we need to estimate the artifactual timecourses $\{\mathbf{a}_k\}$ and their weights ($w_{k,v}$)
1180 so that we can subtract them out. If the artifactual components $\{\mathbf{a}_k\}$ were uncorrelated with the
1181 sound-driven responses (\mathbf{s}_v) we could estimate them by performing CCA on voxel responses from
1182 inside and outside of cortex, since only the artifacts would be correlated. However, we expect
1183 sound-driven responses to be correlated with motion artifacts, and the components inferred by
1184 CCA will thus reflect a mixture of sound-driven and artifactual activity.

1185

1186 To overcome this problem, we first subtract-out the average response of each voxel across
1187 repeated presentations of the same sound ($\dot{\mathbf{d}}_v$). This “recentering” operation removes sound-
1188 driven activity, which by definition is the same across repeated presentations of the same sound:
1189

$$1190 \quad (9) \quad \dot{\mathbf{d}}_v = \sum_k^N \dot{\mathbf{a}}_k w_{k,v}$$

1191

1192 where the dot above a variable indicates its response after recentering (not its time derivative).
1193 Because sound-driven responses have been eliminated, applying CCA to the recentered voxel
1194 responses should yield an estimate of the recentered artifacts ($\dot{\mathbf{a}}_k$) and their weights ($w_{k,v}$) (note
1195 that CCA actually yields a set of components that span a similar subspace as the artifactual
1196 components, which is equivalent from the perspective of denoising). To simplify notation in the
1197 equations below, we assume this estimate is exact (i.e. CCA exactly returns $\dot{\mathbf{a}}_k$ and $w_{k,v}$).

1198

1199 Since the weights ($w_{k,j}$) are the same for original (\mathbf{d}_v) and recentered ($\dot{\mathbf{d}}_v$) data, we are halfway
1200 done. All that is left is to estimate the original artifact components before recentering (\mathbf{a}_k), which
1201 can be done using the original data before recentering (\mathbf{d}_v). To see this, first note that canonical

1202 components are by construction a linear projection of the data used to compute them, and thus,
1203 we can write:

$$1204 \quad (10) \quad \mathbf{a}_k = \sum_v^V \dot{\mathbf{d}}_v \beta_{k,v}$$

1205
1206 We can use the reconstruction weights ($\beta_{k,v}$) in the above equation to get an estimate of the
1207 original artifactual components by applying them to the original data before recentering:
1208

$$1209 \quad (11) \quad \mathbf{a}_k \approx \sum_v^V \mathbf{d}_v \beta_{k,v}$$

1210
1211 To see this, we expand the above equation:
1212

$$1213 \quad (12) \quad \sum_v^V \mathbf{d}_v \beta_{k,j} = \sum_v^V \left(\sum_{k'}^N \mathbf{a}_{k'} w_{k',v} + \mathbf{s}_v \right) \beta_{k,v}$$

$$1214 \quad (13) \quad = \sum_{k'}^N \mathbf{a}_{k'} \sum_v^V w_{k',v} \beta_{k,v} + \sum_v^V \mathbf{s}_v \beta_{k,v}$$

1215
1216 The first term in the above equation exactly equals \mathbf{a}_k because $w_{k',v}$ and $\beta_{k,v}$ are by construction
1217 pseudoinverses of each other (i.e. $\sum_v^V w_{k',v} \beta_{k,v}$ is 1 when $k' = k$ and 0 otherwise). The second
1218 term can be made small by estimating and applying reconstruction weights using only data from
1219 outside of cortex, where sound-driven responses are weak.
1220

1221 We thus have a procedure for estimating both the original artifactual responses (\mathbf{a}_k) and their
1222 weights ($w_{k,j}$), and can denoise our data by simply subtracting them out:
1223

$$1224 \quad (14) \quad \mathbf{d}_v - \sum_k^K \mathbf{a}_k w_{k,v}$$

1225
1226 **Procedure.** We now give the specific steps used to implement the above procedure using matrix
1227 notation. The inputs to the analysis were two matrices (D_{in}, D_{out}), each of which contained voxel
1228 responses from inside and outside of cortex. Each column of each matrix contained the response
1229 timecourse of a single voxel, concatenated across all sounds and repetitions (i.e. \mathbf{d}_v in the above
1230 derivation). We also computed recentered data matrices ($\dot{D}_{in}, \dot{D}_{out}$) by subtracting out trial-
1231 averaged activity (i.e. $\dot{\mathbf{d}}_v$).
1232

1233 CCA can be performed by whitening each input matrix individually, concatenating the whitened
1234 data matrices, and then computing the principal components of the concatenated matrices (de
1235 Cheveigné et al., 2019). Our procedure is an elaborated version of this basic design:
1236

1237 1. The recentered data matrices were reduced in dimensionality and whitened. We implemented
1238 this step using the singular value decomposition (SVD), which factors the data matrix as the
1239 product of two orthonormal matrices (U and V), scaled by a diagonal matrix of singular values (S):
1240

$$1241 \quad (15) \quad \dot{D}_{in} = \dot{U}_{in} \dot{S}_{in} \dot{V}_{in}$$

$$1242 \quad (16) \quad \dot{D}_{out} = \dot{U}_{out} \dot{S}_{out} \dot{V}_{out}$$

1243

1244 The reduced and whitened data was given by selecting the top 250 components and removing
1245 the diagonal S matrix:

1246

$$1247 \quad (17) \quad \dot{D}_{in-white} = \dot{U}_{in}[:,1:250]\dot{V}_{in}[1:250,:]$$

$$1248 \quad (18) \quad \dot{D}_{out-white} = \dot{U}_{out}[:,1:250]\dot{V}_{out}[1:250,:]$$

1249

1250 2. We concatenated the whitened data matrices from inside and outside of cortex across the voxel
1251 dimension:

1252

$$1253 \quad (19) \quad \dot{D}_{cat} = [\dot{D}_{in-white}, \dot{D}_{out-white}]$$

1254

1255 3. We computed the top N principal components from the concatenated matrix using the SVD:

1256

$$1257 \quad (20) \quad \dot{D}_{cat} = \dot{U}_{CC}\dot{S}_{CC}\dot{V}_{CC}$$

1258

1259 \dot{U}_{CC} contains the timecourses of the canonical components (CCs), ordered by variance, which
1260 provide an estimate of the artifactual components after recentering (i.e. $\hat{\mathbf{a}}_k$). The corresponding
1261 weights (i.e. $w_{k,v}$) for voxels inside of cortex were computed by projecting the recentered data
1262 onto \dot{U}_{CC} :

1263

$$1264 \quad (21) \quad W_{in} = \dot{U}_{CC}^+ \dot{D}_{in}$$

1265

1266 where + indicates the matrix pseudo-inverse.

1267

1268 4. The original artifactual components before recentering (i.e. \mathbf{a}_k) were estimated by learning a
1269 set of reconstruction weights (B) using recentered data from outside of cortex, and then applying
1270 these weights to the original data before recentering:

1271

$$1272 \quad (22) \quad B = \dot{D}_{out}^+ \dot{U}_{CC}$$

$$1273 \quad (23) \quad U_{CC} = D_{out} B$$

1274

1275 U_{CC} is an estimate of the artifactual components before recentering (i.e. \mathbf{a}_k).

1276

1277 5. Finally, we subtracted out the contribution of the artifactual components to each voxel inside of
1278 cortex, estimated by simply multiplying the component responses and weights:

1279

$$1280 \quad (24) \quad D_{denoised} = D_{in} - U_{CC} W_{in}$$

1281

1282

1283 **Simulation.** We created a simple simulation to test our method. We simulated 1000 voxel
1284 responses, both inside and outside of cortex, using equation 8. For voxels outside of cortex, we
1285 set the sound-driven responses to 0. We also added voxel-specific noise to make the denoising
1286 task more realistic/difficult (sampled from a Gaussian). Results were very similar across a variety
1287 of noise levels.

1288

1289 To induce correlations between the artifactual (\mathbf{a}_k) and sound-driven responses (\mathbf{s}_v), we forced
1290 them to share a subspace. Specifically, we computed the sound-driven responses as a weighted
1291 sum of a set of 10 component timecourses (results did not depend on this parameter), thus forcing
1292 the responses to be low-dimensional, as we found to be the case:

1293

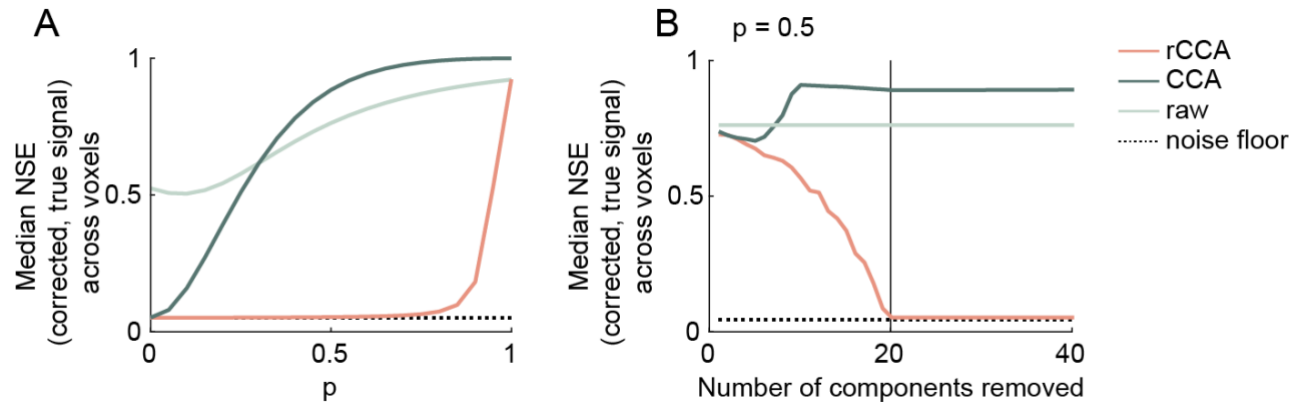
1294 (25)
$$\mathbf{s}_v = \sum_{j=1}^{10} \mathbf{u}_j m_{j,v}$$

1295
1296 The artifactual timecourses were then computed as a weighted sum of these same 10
1297 components timecourses plus a timecourse that was unique to each artifactual component:
1298

1299 (26)
$$\mathbf{a}_k = p \sum_{j=1}^{10} \mathbf{u}_j n_{j,k} + (1 - p)\mathbf{b}_k$$

1300
1301 where p controls the strength of the dependence between the sound-driven and artifactual
1302 components with a value of 1 indicating complete dependence and 0 indicating no dependence.
1303 All of responses and weights (\mathbf{u}_j , \mathbf{b}_k , $m_{j,v}$, $n_{j,k}$) were sampled from a unit-variance Gaussian.
1304 Sound-driven responses were constrained to be the same across repetitions by sampling the
1305 latent timecourses \mathbf{u}_j once per sound, and then simply repeating the sampled values across
1306 repetitions. In contrast, a unique \mathbf{b}_k was sampled for every repetition of every sound to account
1307 for the fact that the artifacts like motion will vary from trial-to-trial. We sampled 20 artifactual
1308 timecourses using equation 26.

1309
1310 We applied both standard CCA and our modified rCCA method to the simulated data. We
1311 measured the median NSE between the true and estimated sound-driven responses (\mathbf{s}_v),
1312 computed using the two methods as a function of the strength of the dependence (p) between
1313 sound-driven and artifactual timecourses (**Fig A1A**). For comparison, we also plot the NSE for
1314 raw voxels (i.e. before any denoising) as well as the minimum possible NSE (noise floor) given
1315 the voxel-specific noise (which cannot possibly be removed using CCA or rCCA). When the
1316 dependence is low, both CCA and rCCA yield similarly good results, as expected. As the
1317 dependence increases, CCA performs substantially worse, while rCCA continues to perform well
1318 up until the point when the dependence becomes so strong that sound-driven and artifactual
1319 timecourses are nearly indistinguishable. Results were not highly sensitive to the number of
1320 components removed as long as the number of removed components was equal to or greater
1321 than the number of artifactual components (**Figure A1B**).



1322
1323 **Figure A1:** Simulation results. **A.** Median NSE across simulated voxels between the true and
1324 estimated sound-driven responses (s_v), computed using raw/undenoised data (light green line),
1325 standard CCA (dark green line), and recentered CCA (red line). Results are shown as a function of
1326 the strength of the dependence (p) between sound-driven and artifactual timecourses. The minimum
1327 possible NSE (noise floor) given the level of voxel-specific noise is also shown. **B.** Same as panel A,
1328 but showing results as a function of the number of components removed for a fixed value of p (set to
1329 0.5).
1330